NAZARBAYEV UNIVERSITY

School of Engineering and Digital Sciences

Department of Mechanical and Aerospace Engineering

MSc Thesis

DESIGN OF GRAPENE MEMBRANE FOR WASTEWATER TREATMENT

By Stephen UmaOji

Supervisors: Professor Konstantinos Kostas and Assistant Professor Yerbol Sarbassov

This MSc thesis submitted to Nazarbayev University in partial fulfillment of the requirements for the degree of Master of Science in Mechanical and Aerospace Engineering

May 2026

DECLARATIOION

I hereby, declare that this manuscript, entitled "*The Design of Graphene membrane for waste water treatment using Machine learning*", is the result of my own work except for quotations and citations, which have been duly acknowledged.

I also declare that, to the best of my knowledge and belief, it has not been previously or concurrently submitted, in whole or in part, for any other degree or diploma at Nazarbayev University or any other national or intentional institution.

……

NAME: UMAOJI STEPHEN

22/04/2026

ABSTRACT.

The growing global need for fresh water has driven the development of advanced membrane technologies with not only high-water permeability but also good rejection of contaminants and long-term operational stability. Graphene-based membranes have been considered as the promising candidate for next-generation water purification because of its atomic thickness, high mechanical strength and tunable nanoporous structure. We present here a study of the performance of various functionalized graphene nanopore membranes in water treatment via MD simulations. Two broad strategies for functionalization were explored: uniform surface functionalization, and pore-edge functionalization. Three different chemical groups, hydrogen (H), fluorine (F), and amine (NH_2) were chemically functionalized on graphene membranes at different levels of functionalization. Functionalization was implemented uniformly over the surface at a coverage of 20%, and pore-specific functionalization localized to regions around the edges of the nanopore at a coverage of 15%. The simulation system includes the pressure-driven water through graphene nanopores helping remove of contaminants such as $PFBA^-$ anions and Pb^{2+} ions. Molecular dynamics simulations were carried out using the LAMMPS simulation package with explicit water models and realistic intermolecular interaction parameters. To accelerate transport processes, they were subjected to a piston-driven pressure of 20,000 bar and the resulting flux values were scaled to realistic operating pressures of 100 bar. These results show that pore chemistry is a key parameter in determining membrane transport behavior. Also, Fluorinated graphene membranes achieved the highest water flow rates since their reduced friction and hydrophobicity of channel structure favor almost frictionless transport of water in the nanopore. The permeability was a bit lower for hydrogen-functionalized membranes, but the transport properties remained stable. Fouling index analysis suggested that pore functionalization could generally reduce fouling

relative to uniform functionalization owing to localization of chemical groups in proximity to the nanopore region which mitigates surface-wide contaminant adsorption. Electrostatic interactions occurring between the functional groups and charged species such as heavy metal ions and PFAS compounds are the primary driving mechanism for selectivity. Pore-functionalized membranes exhibited the best balance of desirable characteristics (high water flux, strong rejection, reduced foulant deposition tendency) among the studied systems.

Acknowledgement

I must give special thanks to my supervisor, Professor Konstantinos Kostas, for his encouragement and support – with readiness to always lead and correct in the right direction; whose contributions has brought the research work up to standard, so content look more like what obtains in a typical membrane study.

Also, I won't fail to give many thanks to Dr Hamed M. Amin and Narges Vafa for their support in directing me to kickstart this project as their experience and contributions in this area of computational material science gave me the zeal to venture with confidence.

TABLE OF CONTENT

LIST OF ABBREVIATIONS AND SYMBOLS

CMS	Computational material science
MD	Molecular Dynamics
LAMMPS	Large scale Atomic and molecular Massively Parallel Simulator
LJ	Lennard jones potential
G -F15	Graphene with 15% uniform functionalization using Fluorine
G-H15	Graphene functionalized with 15% Hydrogen
G- HN2-15	Graphene membrane functionalized with 15% amine group
G- F20	Graphene membrane functionalized with 20% Fluorine group
FI	Fouling index
R	Rejection

LIST OF TABLES

LIST OF FIGURES

CHAPTER 1

INTRODUCTION

1.1 BACKGROUND STUDY AND OVERVIEW

Many techniques exist for treating water, however because of global population explosion and coupled with industrialization, some toxic and emerging pollutants have evolved – arising from the use of domestic paints for buildings and foams from firefighting equipment to the exhaust of automotive engines which contains incomplete combustion mixtures of charred fuel with oil additives. All these combines in the water cycle and find their way to streams and oceans where they pollute the water table[1]. These class of pollutants are emergent, that is not the regular type of pollutants that are easily removed by traditional techniques hence require a modern method[2]. Per and poly Fluoro Alkyl Sulfonates (PFAS) are in this class of emergent pollutants known as “forever chemicals” which are at the center of research because of their toxicity and persistency in the environment. They comprise an expanse of fluorinated surfactants that consist of thousands of derivatives. Some of the popular few are:

- PFOA; Perfluoro octanoic acid, $C_7F_{15}COOH$, an 8- carbon chain fluorinated carboxylic acid that has been used in making fluoropolymers and Teflon. They are highly carcinogenic and can cause developmental issues with immune system alterations.
- PFOS; Perfluoro-octanoic sulfonates, with chemical formula $C_8F_{17}SO_3^-$. It is widely used as firefighting foam and as stain removers.
- PFNA; Perfluoro nonanoic Acid
- PFBS; perfluoro butane sulphonic acid

- perfluoro hexane sulfonic acid (PFHxS) and
- GenX; technically known as hexafluoropropylene oxide dimer acid (HFDO-DA) are next generation contaminants derived from the first two but are still being categorized. The first two are usually highly regulated by different countries and have been widely studied.

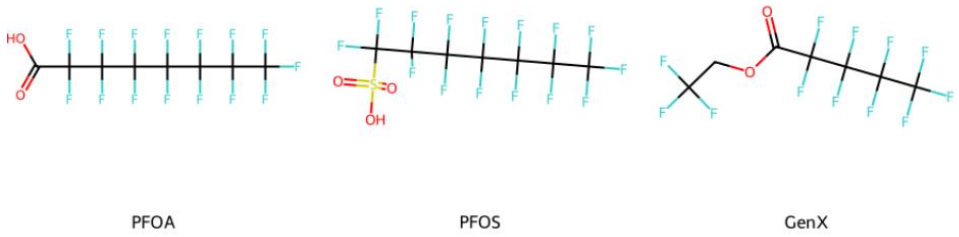

Fig 1.1: structure of popular per fluoro Alkyl substances derivatives.

They exhibit amphiphilicity – they have hydrophilic polar heads and hydrophobic fluoroalkyl tails. This ensures tough adherence to surfaces of membranes and can partition strongly to interfaces, thus decreasing the membranes resistance to fouling.

Several graphene and graphene derivatives (Graphene oxides, fluorographene, graphene-based composites- polymer graphene nanocomposites, Metal oxide framework (MOF)/graphene network etc.) have been used in wastewater research because of their tunable chemistry, strength and robustness, and their precise separation in nanochannels. Even with all this manipulation of graphene features, removal of nano-sized PFAS while preventing membrane fouling still proves difficult[3].

Molecular dynamics is well positioned to accurately define the water treatment modelling for enabling surface design, wetting, translocations and atom drivers in absorption. The results of

MD can give sufficient information on contact angle calculations, chain length, functional group, pore, headgroup chemistry etc. – which can further lend itself as variables for optimization.

The increase of PFOA, PFOS and GenX pollutants are stringently regulated by many countries because of their toxicity and cancerous nature– "regulated" means they cannot exceed beyond some set concentration called maximum contamination Limit (MCL) in portable water, else the water is labeled unsafe for human use. In April 10, 2024, the US Environmental protection Agency set the maximum concentration levels (MCLs) of PFOA and PFOS in drinking water should not exceed 4 ng/L, while the MCLs for PFHxS, PFNA, PFBS, and GenX should not exceed 10 ng/L. Traditional wastewater remediation programs – flocculation and coagulation, ion exchange, activated carbon, and advanced oxidation - have limited capability in removing PFAS and heavy metals[4]: use of sorbents to absorb PFAS fail even for the short-chained ones in ionic solutions and heavy metals remediation suffers from membrane fouling and selectivity problems. Fouling gives rise to a reduced wettability and affects flux. Multivalent ions also hinder permeability, thus generally degrading performance. Also, heavy metals, being increasingly deposited as waste from industries, are of concern[5]. Major heavy metal found dissolved in wastewater are Mercury (Hg^{2+}), cadmium (Cd^{2+}), and arsenic (As^{3+}) which are toxic, non-biodegradable and usually accumulates in the body over time causing endocrine disruptions[5], [6]. The two groups of contaminants are now globally known as "emerging contaminants" which require urgent solutions for their absorption and degradation[7].

Over the decades, experimental tools have aided the indirect solutions for binding and fouling but have not addressed issues like ion pairing, hydrogen bonding, pi-pi interactions which occur at nanoscale, and this is where MD has been very successful in providing significant results[8], [9], [10]. MD can simulate transport of PFAS and metals under dynamic absorption,

contact angles and surface free energies. Major research work has been in MD simulations for PFAS remediation alone[11], [12], [13], [14]or simulations for heavy metal removal[15], with none working on a combination of remediation of PFAS and heavy metals except for Loganathan et al[14] combining multiple PFAS in one box (but not PFAS plus a heavy metal).

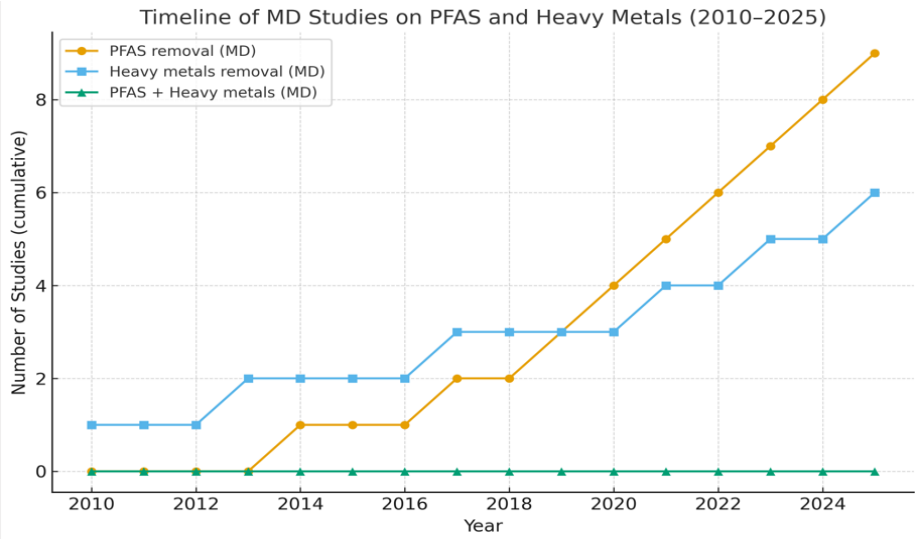

Fig 1.2; studies on PFAS, heavy metals using MD analysis with little or no study done on PFAS+ Heavy metals.

Also another curative search by Ma and Chew[16], the number of publications on fouling analysis using MD increased exponentially from 1995 to 2024. This also shows the eagerness to offer urgent solutions on the subject matter of water treatment.

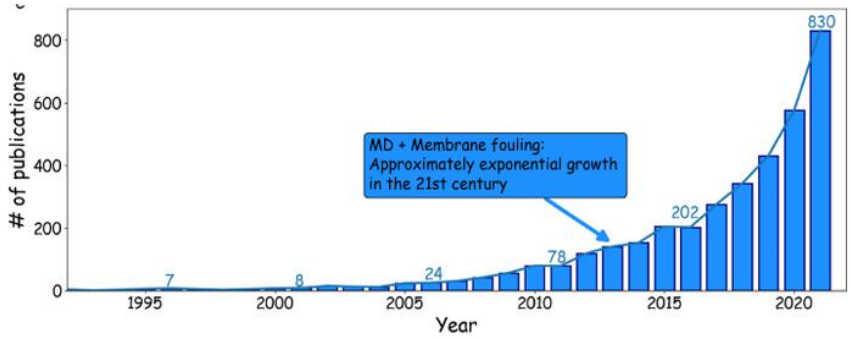

Fig 1.3: shows exponential increase of research on fouling using MD technique.

Other contaminants that appear in water treatment are Cadmium from used batteries, Mercury, Arsenic, chromium and lead which come from old water pipes and some other trace elements. These heavy metals present in the water are toxic and pose a threat to health causing cancer, endocrine disruption, kidney and other organ failure[17].

This thesis work will consider a case where PFAS together with heavy metal is rejected, to make it a unique work. Lead will be used as the model heavy metal for remediation studies alongside Per fluoro Butanoic Acid (PFBA), a type of PFAS, removal.

1.2 MOTIVATION

The main motivation behind this project comes from the research project on graphene membrane for wastewater treatment managed by my supervisor, the researcher was involved as a research assistant. In earlier work, computational techniques were used to design a graphene membrane, with methyl functionalization. Chosen target variables were Youngs modulus, thermal conductivity, thermal stress and thermal strain. However, in this thesis project, properties specific to the graphene which affects it during usage have been chosen; Water-flux, adsorption, rejection and fouling index. Similar techniques used in the project work ranging from design of the

graphene sheets using python codes to running LAMMPS simulations to obtain results of selected output has been employed. Also, earlier research assistant work investigated the linearized relationships between different percentages of functionalization producing specific set of target values which was then used to train the system to arrive at machine - learned predictions of the best membrane functionalization for the material. This stage is usually data-hungry and takes a lot of computational time, thus I was not incorporated because of time constraints. However, the MD values and plots obtained were used to deduce the membrane of choice that meets the best values of the target variables and MD derived results will be employed to develop the Machine learning studies later.

1.3 RESEARCH OBJECTIVES

As PFAS and heavy metals have continued to be a challenge in designed membranes during water treatment, there's a call for a more robust membrane design for the complete remediation of these pollutants while at the same time have minimized fouling. Graphene and graphene-based membranes have been used in different materials field of study – in superconductors, battery, sensors, gas separation etc.[18]- because of their improved mechanical strength relative to other membranes, tunable pore size, and ease of doping and functionalization their usage has not been developed for fouling conditions per PFAS and heavy metal. MD offers an opportunity to make this study to build membranes for strong antifouling resistance with high rejection of PFAS and lead (Pb) metal.

Hence the goal is to design a graphene based functionalized membrane for high water flux, low fouling and adsorption with a high rejection ratio of PFAS and lead contaminants with a minimum fouling property.

1.3.1 Sub-objectives

- Design model of functionalized graphene-based membranes
- Study the rejection mechanisms and transport of these pollutants: PFAS and Lead.
- Simulate fouling dynamics with respect to PFAS and lead compound and investigating their effects on functionalization and permeate flux, Adsorption energy and rejection.
- Lastly identify chemical and structural modifications that minimize fouling maximize rejection of PFAS., with a high-water flux. Fig 4 shows the summary of objectives to be done.

Fig 4: sub-objective workflow

CHAPTER 2

LITERATURE REVIEW

2.1 EXPERIMENTAL STUDY

Membrane technology is one of the most effective methods for desalination, water purification, biomedical applications and gas separation because of its ease of operation and energy efficiency. A part of membrane technology is graphene-based membranes have attracted scientific attention due to graphene's tunability and atomic thickness, chemical stability, high mechanical strength, with a unique transport property. Experimental investigations have revealed that graphene oxide (GO), functionalized graphene membranes and reduced graphene oxide (rGO) are superior in terms of performance than conventional polymeric membranes with respect to permeability and selectivity[19]. Graphene-based membranes also showed better fouling resistance compared to polymeric membranes. This thesis reviews experimental developments in the synthesis of graphene membranes, their functionalization strategies, and material characterization methods.

2.1.1 Graphene membrane synthesis

The synthesizing graphene membranes generally starts with the preparation of graphene or graphene oxide nanosheets. One of the most popular methods is the Hummers' oxidation method, where sulfuric acid and potassium permanganate is used to oxidize graphite to form graphene oxide [20]. GO contains oxygenated radical group functionality, which improves dispersion in water and ensures ease of membrane fabrication. Fig 2.1 illustrates the synthesis

process.

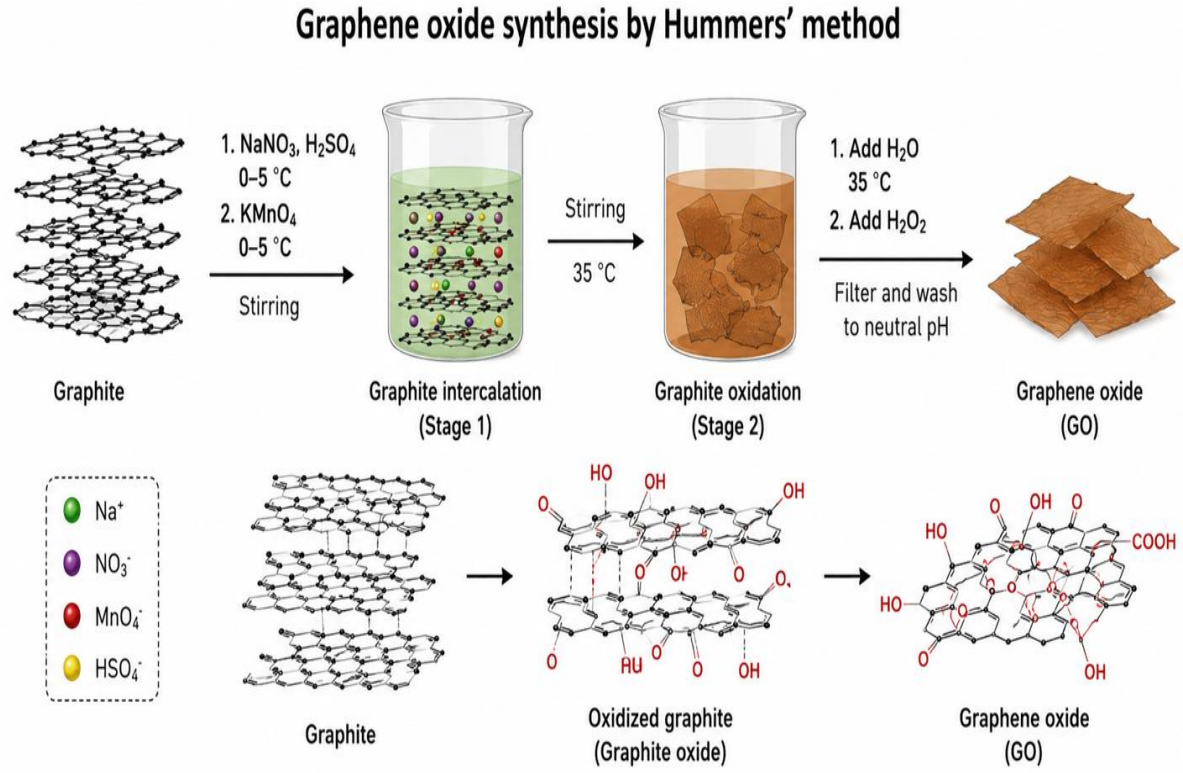

Fig 2.1 showing graphene synthesis by hummer's method.

These GO sheets are then exfoliated into one- layer or few-layer nanosheets by using ultrasonic vibrations at desirable frequency.

There are other membrane fabrication techniques available: Vacuum filtration:

Involves using porous support to filter a GO suspension (e.g. a polymer substrate or an aluminum oxide), thus allowing for the formation of a stacked layer. This technique allows for highly ordered nanochannels.

Spin coating: GO solution is rotated in a sprayed substrate to create uniform and thin films with desired thickness.

Dip coating and Spray coating: Used for scalable industrial fabrication on ceramic or polymer supports. Layer-by-layer assembly: Alternating deposition of oppositely charged materials

enables precise control of membrane architecture. One pioneering experimental study showed that atomic-thick GO sheets were impermeable to gases such as helium but permitted rapid influx of water vapor. This unusual selectivity was attributed to two-dimensional capillaries formed between the stacked GO sheets[20].

2.1.2 Functionalization of Graphene Membranes Although pristine graphene has good dispersion properties, it is hydrophobic in nature and difficult to process. Thus, it is necessary to functionalize it to improve hydrophilicity, interlayer spacing, chemical affinity, and membrane stability.

(a) Oxygen Functionalization GO itself is a functionalized derivative of graphene which has the oxygen radical present. These oxygen containing radicals boost water affinity, hence its hydrophilicity and help create paths for transport channels for polar molecules. Williams et. al. [21] have shown that controlling the extent of oxidation during the synthesis of GO laminates significantly affects transport properties and rejection performance.

(b) Carboxyl Functionalization graphene acid membranes that are rich in carboxyl functional group radicals have been synthesized through many oxidation routes. For the first time Khorramadel et. al.[22] synthesized graphene acid membrane. These membranes are known for their negative surface charge, better hydrophilicity, and improved salt rejection compared with pristine GO membranes. The study reported water flux of 73.2 $L \cdot m^{-2} \cdot h^{-1}$ with high sulfate rejection.

(c) Amine Functionalization 11 Introducing ethylenediamine between GO layers to crosslink the laminates results in the addition of amine functional groups. This enhances mechanical dimensional stability, prevents membrane swelling, and improves rejection. Amine groups can also provide adsorption sites for heavy metals.

(d) Polymer Composite Functionalization GO can be combined with polymers such as polyamide, polysulfone, chitosan, and polyvinyl alcohol. These hybrid membranes combine polymer flexibility and low cost with graphene high flux, high selectivity with their improved antifouling properties [23].

(e) Metal-Ion Crosslinking Using metal cations to stabilize GO membranes by forming metal – cross-linkages offers an improved structural integrity in aqueous solutions due to interactions with carboxy group. Cations like Ca^{2+}, Al^{3+}, and Mg^{2+} are frequently used.

2.1.3 Material characterization of Graphene membranes

Validating synthesized membranes to study properties and performance requires detailed chemical, structural, and performance characterization. Xu et. al.[24] discusses usage from (a) to (h) as below:

(a) Transmission Electron Microscopy (TEM) TEM ensures high resolution nanoscale imaging of graphene sheets is made, checks integrity of the laminates, quality of pore formation investigated, and interlayer spacing. It also confirms exfoliation quality.

(b) Scanning Electron Microscopy (SEM) 12 SEM is used to observe membrane surface morphology and cross-sectional layered structures. It reveals stacking order, wrinkles, cracks, and membrane thickness.

(c) Fourier Transform Infrared Spectroscopy (FTIR) FTIR is used to identify oxygenated functional groups such as carboxyl, hydroxyl and epoxy groups, which confirms presence of oxidation and type of functional group present.

(d) X-ray Diffraction (XRD) XRD is important for determining interlayer spacing. The spacing in GO membranes can be increased by hydration, which directly influences permeability.

(e) Raman Spectroscopy Raman spectra show the D-band and G-band the shows presence of defects in the graphene and graphite ordering. The ID/IG ratio is usually used to show extent of disorder after oxidation.

(f) X-ray Photoelectron Spectroscopy (XPS) XPS provides elemental composition and bonding states. It quantifies C/O ratio and confirms the presence of nitrogen, sulfur, fluorine, or metals after functionalization.

(g) measuring contact angle Surface wettability is a measure of the hydrophilicity or hydrophobicity of the membrane, and water contact angle measurements scales them appropriately; a high contact angle (the angle the liquid surface makes with the horizontal) signifies a hydrophobic surface or membrane. An angle over 135 degrees exhibits superhydrophobicity. Lower contact angles between 0 and 30 degrees indicate hydrophilic membranes favorable for water permeation. The angle of 0 degrees is superhydrophilic[25].

(h) Mechanical Testing Tensile strength, thermal conductivity and Young's modulus measurements evaluate membrane mechanical properties and durability. Graphene membranes generally exhibit better mechanical strength compared with polymeric membranes.

2.2 COMPUTATIONAL STUDY.

Several works using MD have been investigated on graphene and graphene-based membranes to check variables like absorption strength and diffusion coefficients, pollutant rejection, fouling etc. Outside wastewater modelling, MD has been used to simulate various biological, chemical, biophysical and thermomechanical processes such as LAMMPS (Large-scale

Atomic Molecular Massively Parallel Simulator)[26], GROMACS, NAMD, DE_POLY, CHARMM, open MM are the popular ones. However the mostly used are LAMMPS, NAMD and GROMACS[27]. Typically, all MD simulations begin with scripts for an input file, which must be in a given file format (.pdb..gro,.data etc.) [1]. Tools are available for creating inputs to MD like VMD or Avogadro, ASE, PACKMOL, MOL Template, MBuild and foyer. These dedicated input tools have added in obtaining input data files for modeling close to reality physical processes while essentially performing energy minimizations (because atomic positions are solved as an optimization problem to minimize distance between them) and preventing overlapping atoms before simulations[28].The workflow from for MD simulations can be summarized in the figure below.

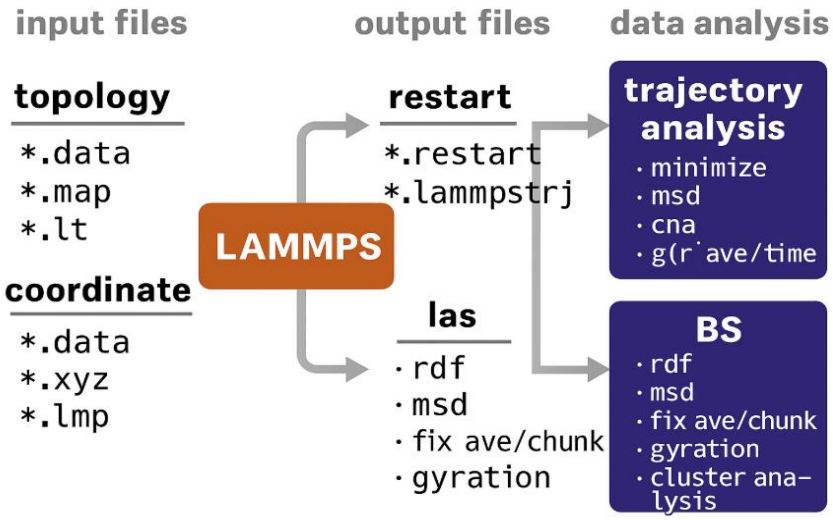

Fig 2.2: LAMMPS workflow from input to output

Awawdeh et al[29] MD techniques in investigating the absorption strengths and diffusion coefficients of all the PFAS analogues. The result gave that adsorption increased with molecular weights. PFOS has the highest weight of 500 g/mol and showed the strongest absorption energy of (-171kCals/mol). Also, effect of diffusion was also investigated. It was also shown that the

sulfonic heads also affected the absorption- compounds with acid head groups had better interaction with the graphene membrane than those with carboxylic heads. Diffusion study was also done and increased with carbon chain length. The PFNA diffused fastest.

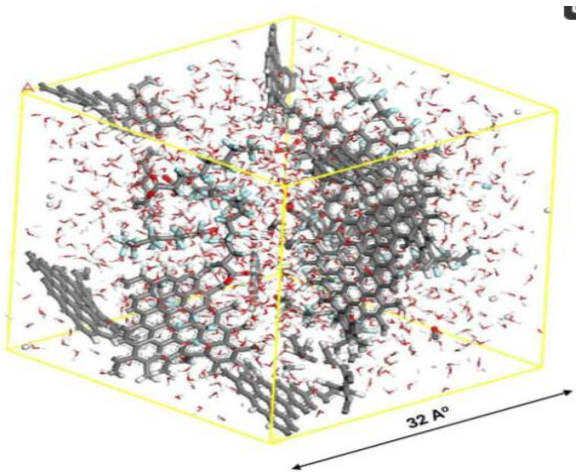

Fig 2.3: Amorphous cell of PFOA compound. Source: Adapted from[29]

In a related work by Bresnahan et al[1], they varied the type of functionalization of the graphene- obtaining 5 different graphene functionalized structures including fully fluorinated pristine graphene; Graphene oxide fully-fluorinated, partially fluorinated, amine and amide functionalized graphene functionalized flakes to investigate which of the material removes PFAS the fastest, that is has the best PFAS adsorption – the PFAS analogues were all used for this computational analysis –PFBA,PFOA and PFOS.

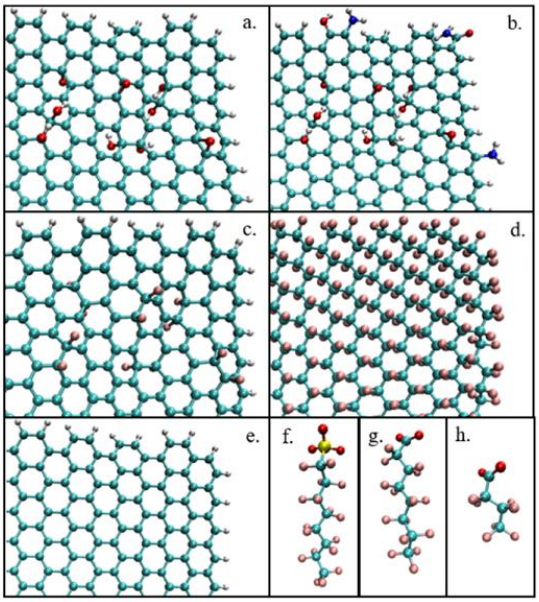

Fig 2.4: Functionalized graphene types. Source: Adapted from [1]

. Structure of the materials under study a) graphene oxide (GOX), b) amine- and amide-graphene oxide (AGO), c) partially fluorinated graphene flake (GFL), d) fully fluorinated graphene flake (FFL) e) pristine graphene (GNX) f) anionic perfluoro octane sulfonic acid (PFOS), g) anionic perfluorooctanoic acid (PFOA), h) anionic Perfluoro butanoic acid (PFBA).Source: Adapted from[2].

Their result showed that PFAS adsorption decreases in the order: pristine graphene (fully fluorinated) graphene oxide, (partially fluorinated) amine and amide functionalized graphene oxide flake. That is pristine graphene being the best material for PFAS removal. The long-chained PFAS are much more easily adsorbed compared to the short-chained ones, with the sulfonate head adsorbed faster than the carboxylic heads. This derivation is in tune with work done by Awawdeh etal [1]. They computed various linear interaction energies with the flake and flake, flake and water, and flake water and type of PFAS (PFBA, PFOA and PFOS).

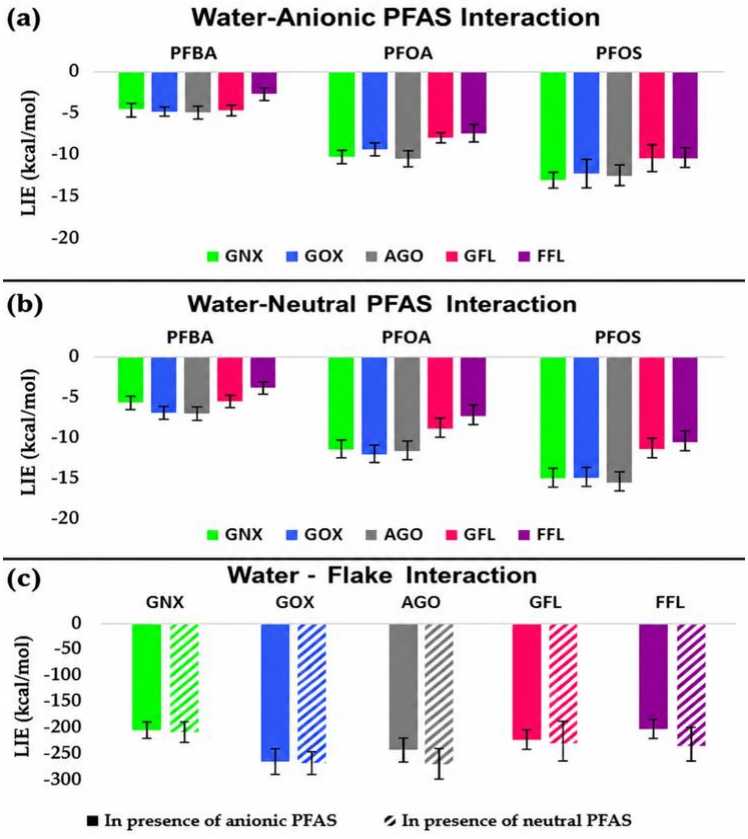

Fig 2.5: Linear interaction energies between water and functionalized material. Source: Adapted from [1].

Binazir et al [15],in another MD research, investigated the efficiency of removing mercury (Hg2+) and Arsenic (As3+)at a concentration of 0.5M using graphene oxide membrane. First, Packmol and Python were used to model the membrane, ions and water with the system being modelled in a simulation box. The experiment was conducted in the NPT (Number of atoms, constant pressure and temperature) ensemble for 1 fs using Nose hoover thermostat and barostat. With pressure and temperature set at 1 bar and 298K respectively – this was to keep the unit at room conditions. Then pressure was applied in the x-direction of 200MPaat same ensemble. Same procedure was carried out later by varying temperature variation from 300K to 340K in another simulation. The NVT

ensemble state was run for another 1 ns so to be in equilibrium. Then the dynamic process for heavy metals separation was run for 10ns in the NVT, with solutions to the velocity varlet algorithm using time step of 1 fs. Result showed that when the concentration was increased from 0.5 to 1M, the water flux through the membrane dropped but there was no significant change in ion rejection. Also, when the temperature changed from 300k to 340K the water flux increased with a decreased ion rejection. Furthermore, comparing the process between two membrane types; crossflow and dead-end, the crossflow performed better removing mercury and arsenic ions and also had a better water flux. This work gives insight into what this thesis will involve per the use of MD packages. However, it does not seek to define best operating parameters of the membrane, nor does it consider fouling control.

In selecting membranes many researchers consider fouling index, rejection, adsorption energy and water flux which have also been used as outputs in this computational work. One of the most crucial factors influencing membrane performance is membrane fouling since membrane fouling directly reduces permeability, resistance increases, and membrane life degradation.

2.2.1 Fouling

Fouling is the adhesion and deposition of particles, solutes or microorganisms on the membrane surface or in the pores of membranes that cause a decrease in permeate flux and separation efficiency[30].

Fouling is defined as the accumulation of unwanted material on solid surfaces, with many mechanisms of fouling (e.g. pore blocking, cake layer formation, scaling and biofouling) having differential effects on flux decline and membrane degradation[31].

Fouling index is a quantitative parameter that can be used to evaluate fouling severity and is commonly determined based on flux decline, resistance increase or pressure increase over time. It indicates the level of contamination on the membrane surface and loss of permeability.

Fouling causes an increase in hydraulic resistance due to the formation of a cake layer on the membrane surface that reduces the effective transport area.

The behavior of fouling is largely determined by surface chemistry. Ang, W.S., Lee, S., & Elimelech, M.[32] have showed that hydrophobic membranes have a true tendency toward organic foulants and vice versa due to weak interactions between contaminants on the hydrophilic membrane driving no or less fouling. In another related work, Liu et. al. [33] were able to determine that fouling was highly controlled by electrostatic and membrane foulant interactions. A hydrophilic surface will likely have less fouling than a hydrophobic surface.

Graphene derivatives as membranes have a smoother surface, less roughness, and functional groups that can prevent the adhesion of foulants, resulting in antifouling properties[34]. These special properties make it a preferable choice when compared to polymeric membranes.

Fouling index using resistance-in-series models is usually computed in the following manner:

$$FI = R_f / R_m \quad \ldots\ldots\ldots\ldots\ldots\ldots\ldots\ldots\ldots\ldots\ldots\ldots\ldots 1$$

Where:

R_f is fouling resistance and

R_m the membrane resistance

It means the severity of fouling increases with increase in fouling index.

In molecular dynamics, however, fouling is easily defined as

% area of pore blocked / total pore area.

This allows for easier computation of fouling index[35]

As a result, energy consumption increases due to higher pressure required to maintain flux leading to increased operational costs due to an increase in fouling [10].

Due to their atomically smooth surfaces and reduced surface interaction energy, graphene membranes suppress foulant adsorption and hence lead to lower fouling. Fouling can be reduced by up to 80% with nanoporous graphene membranes compared to polymer membranes.

2.2.2 Water flux

The water flux is expressed as the volume of water that flows through a unit area of the membrane within a given time:

$$J = V / At \quad \ldots\ldots 2$$

Where V/t is the flow rate and A the pore area

Water flux is a key characterization of the productivity and efficiency of membranes. Flux is driven by pressure gradient, pore size and membrane structure. Higher pressure increases the flux until transport is limited by concentration polarization. Homeaigohar et al[34] demonstrated graphene membranes can derive orders of magnitude higher water flux than conventional membranes, due to their slim atomic thickness and presence of nanochannel flow. Due to lowered transport resistance, water permeability orders of magnitude higher than for polymer membranes are attainable in graphene membranes. Transport of water through nanopores is driven by pressure and molecular diffusion, with low friction in the graphene channels.

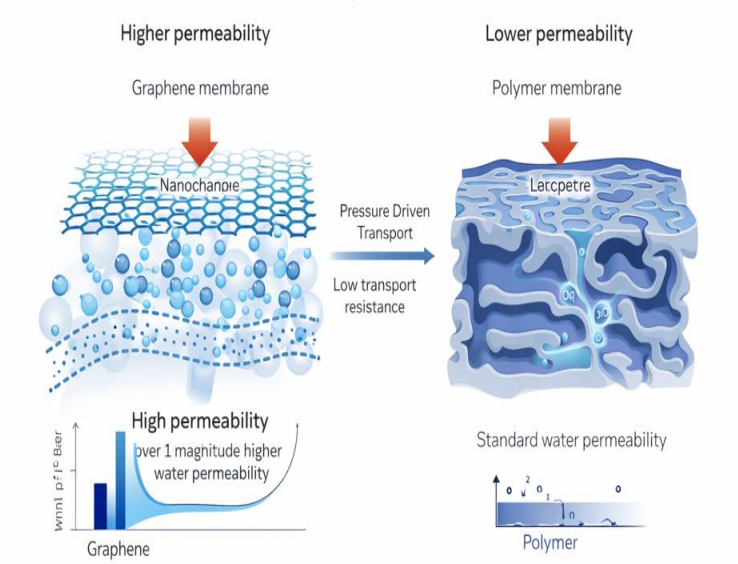

Fig 2.5; Shows graphene performance over polymeric membrane on pressure application.

Fouling and adsorption lead to a decrease in flux over time by blocking pores and increasing resistance.

According to Darcy's law, water flux is proportional to pressure:

$$J = \Delta P \mu / Rj \quad \ldots\ldots 3$$

Where:

ΔP is the pressure difference change

μ the viscosity

Rj = resistance

Low friction and nanoscale confinement effects allow ultrafast water transport through nanoporous graphene membranes. However, this makes computations costly- due to limitations posed by nanoscale transport - as pressure must be simulated over about 1000 bars to get noticeable values of water flux (that is via obtained timestamps of the water count at permeate as the runs progresses)

else a lengthy number of ns runs has to be made. Work done by Xu et. al[24], Qiu et. al[36], Nguyen et al[37] and Cohen- Tanuki et. al. [38] have also used this high pressures.

2.2.3 Rejection

Rejection quantified the ability of a membrane to keep solutes from passing:

$$R = (1 - Cp / Cf) \times 100\ \% \quad \ldots\ldots\ldots\ldots\ldots\ldots\ldots\ldots\ldots\ldots\ldots\ldots\ldots\ldots 4$$

Where:

Cp is the permeate concentration

Cf the feed concentration

High rejection indicates effective separation and is governed by pore size, surface chemistry and electrostatic interactions[39]. Graphene membranes offer high rejection due to atomic-scale pore control and energy barriers for ion transport. Transport of water over particles with sizes comparable to ions, as well as energetics (energy barriers) of the above two mechanisms (size exclusion and energy barrier), can result in rejection of ions from nanoporous graphene materials. Pore size, functionalization, and ion hydration energy greatly impact ion rejection. Graphene membranes can selectively reject up to 97–100% of sodium, which is explained by the nanoscale size of the pores[40].

Low rejection also improves with functionalization because of electrostatic repulsion and repulsion-adsorption effects.

2.2.4 Adsorption Energy

Adsorption of energy determines the strength of interaction between solutes and membrane surface.

Adsorption energy is defined as:

$$E_{ads} = E_{total} - (E_{membrane} + E_{solute}) \quad \text{.....5}$$

Negative adsorption energy indicates strong adsorption.

Adsorption plays a critical role in fouling, rejection, and transport behavior. Strong adsorption increases rejection but may increase fouling. Weak adsorption reduces fouling but may reduce rejection. Graphene membranes exhibit tunable adsorption energy through functionalization. Functional groups such as NH2 increase adsorption through hydrogen bonding. Fluorine functionalization reduces adsorption due to hydrophobic effects. Graphene nanopores provide selective adsorption and rejection properties.

Adsorption of energy determines ion transport barriers and membrane selectivity [41].

Graphene membranes allow water transport while preventing ion adsorption.

Cohen Tanugi and Grossman[38], did an adsorption studies using MD to investigate adsorption energy, transport mechanisms and energy barrier. They found that adsorption affects ion rejection and transport hinderance which is key to influencing fouling and water flux. Zhao et al. in their work using graphene oxide in the presence of lead (Pb2+) saw that adsorption increased in the presence of lead ion which acted binding energy cite with the oxygen functional group in graphene oxide. Thus, presence of competing ions increases the overall adsorption energy which will increase fouling.

CHAPTER 3

METHODOLOGY

3.1 MATERIAL REQUIREMENTS AND DESIGN

The technique to obtain results of molecular dynamics for wastewater membrane filtration studies requires graphene design with functionalization, MD set-up and perform production runs for a period of 0.5ns. Material requirements are:

- Hardware: 8 to 32 core, 32 to 128 RAM GPU
- Software: open source LAMMPS, VMD, Packmol and Atomic Simulation Environment (ASE) and python 3.

3..1.1 Force fields

The unbounded Lennard Jones (LJ) potential will be used to characterize the bond angles and bond lengths of all the atoms used in the simulation, Graphene, Water, lead and chloride ions for balance. The unbounded LJ is given by

$$\sum 4\varepsilon_{ij}\left[\left(\frac{a_{ij}}{r_{\overline{IJ}\cdot}}\right)^{12}-\left(\frac{a_1 j\cdot}{r_{jj}}\right)^{6}\right]-\sum\frac{q_i q_j}{4\prod\varepsilon_0 r_{ij}} \quad \text{.....6}$$

whereεij and σij are the potential well and collision diameter, rij is the distance between atom i and j, qi is the charge of atom i, and $\varepsilon 0$ is the permittivity of vacuum. The LJ parameters and atomic charges can be obtained from various force fields[41]. OPLS-AA forcefield is typically used for graphene. Also, Lemay et. al. [42], used OPLS-AA forcefield in their determination of partitioning constants. Other forcefields like CHARMM36 and AMBER are also used.

3.1.2 Generating the molecules

Avogadro has been used to generate molecules (water, Lead ions, Chloride ions and Polyfluoro Butanoic Acid (PFBA). We have chosen PFBA because, literature has shown, they are the most difficult to absorb because of their short-chained C-C length [1], [3], thus design conditions that lead to their complete adsorption, will eventually adsorb other variants of PFAS easily.

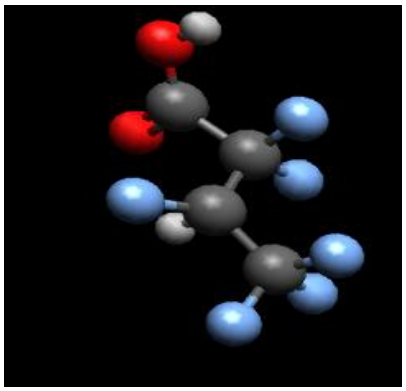

Fig 3.1: PFBA atoms designed in Avogadro

The water molecules have been stabilized to standard bond-length and bond angles using the TIP3P forcefield for water [43].

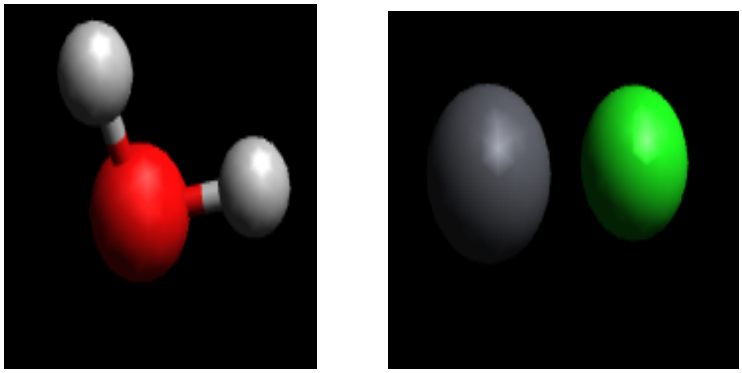

Fig 3.2: left to right Shows Water molecules stabilized to TIP3P model, lead and chlorine atoms.

Lead was used as competing contaminant with PFBA. The anionic form is used because at pH7 (natural water) the hydrogen ion in the carboxylic head deprotonates leaving a negatively charged ion[11], acidifying the solution raises the pH so protonation brings PFBA to its normal state.

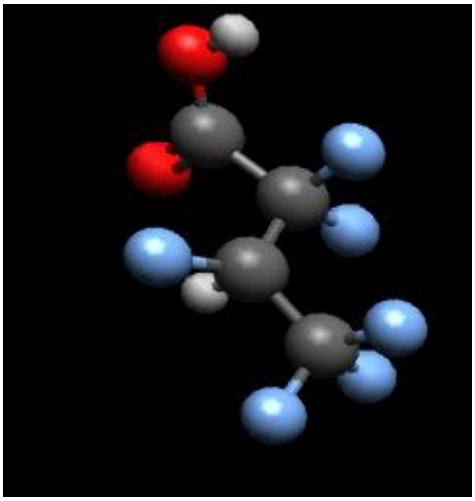

Fig 3.3: Anionized PFBA, designed in Avogadro, with SMILE code from Pub Chem

However, Ligpargen has been used to obtain the LJ coefficients for bonds lengths, angles, dihedrals, charges and harmonics; they can be found in the .lmp file and params file. Changing the

guess values obtained from VMD to the Ligpargen (OPLS AA) values is equivalent to the real physics model that achieves the desired result.

3.1.3 Design of Piston

The piston should have enough capacity to bear the reaction force of the 20,000-bar application pressure. So, a 10 nm square slab 5A thick has been employed. Pure graphene has been used as a material with no other element present to cause any form of doping or functional interference. The thick slabbed piston is placed on top of the fluid mixture surface; it remains fixed during stabilization and minimization. Figure below shows our piston design

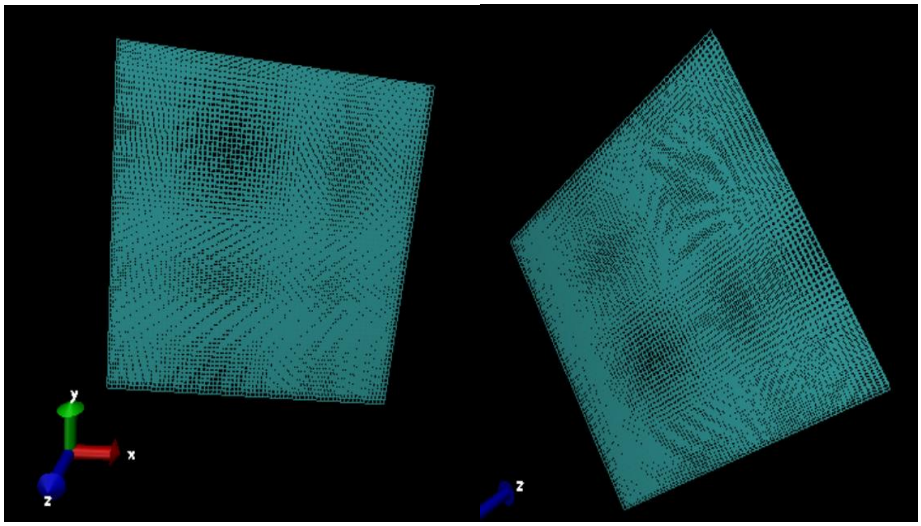

Fig 3,4: piston slab measuring 10nm x 10nm x 0.5nm

3.1.4 Designing the graphene sheet with pore

First the graphene sheet was designed with 3 different functionalization: Hydrogenated graphene, NH2-amine and Fluorized graphene, and one hole created in the middle for membrane adsorption and fouling studies. The sheet has been sized 10nm x 10nm, with hole size of 1.3nm.

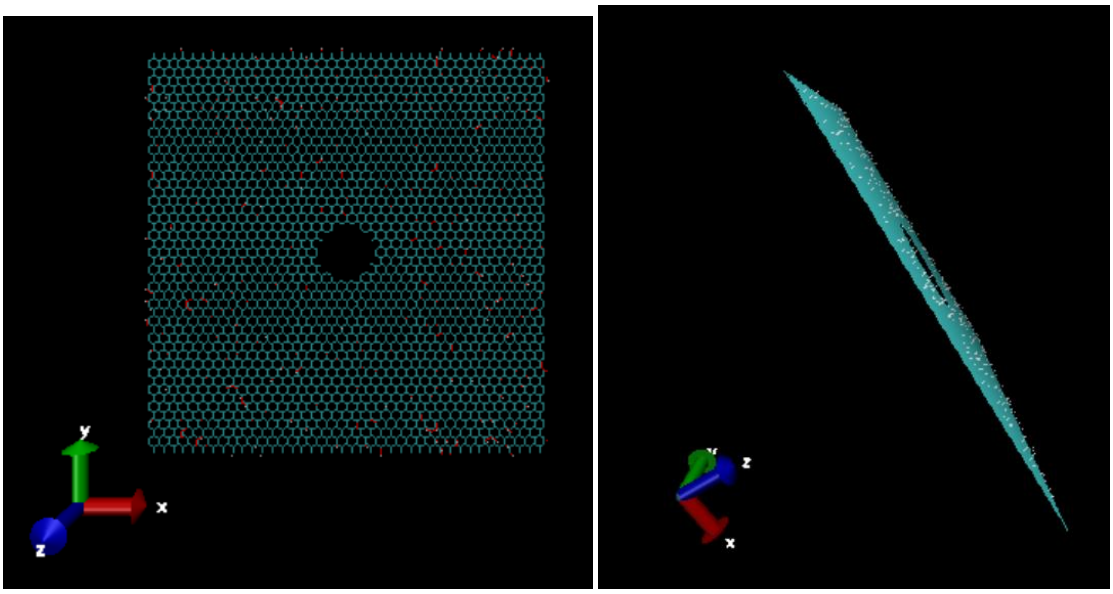

(a) 1.3mm nanopore (b) side view showing surface functionalization

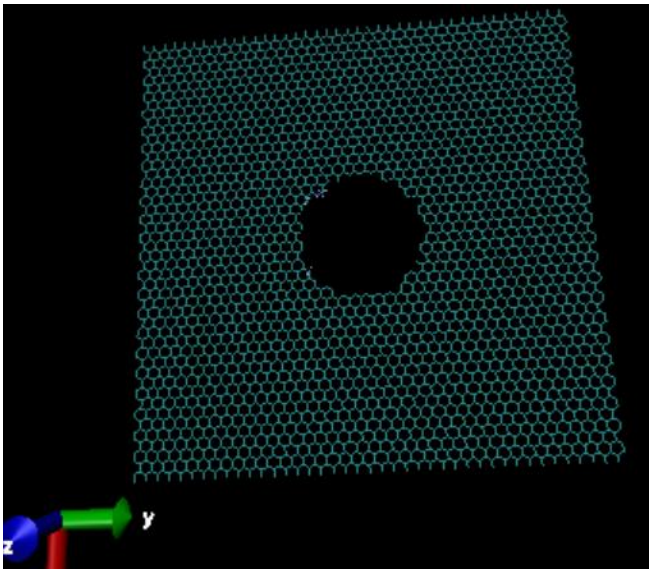

(C) 2.6 nm pore to be used with 20% functionalization for each of H, F and -NH2

Fig 3.5: functionalized graphene with pore size of 1.3nm and doubled

3.1.5 Armchair and zig-zag configuration

The armchair configuration looks like shape of an armchair, hence its name. In this orientation, it across both sublattices symmetrically with the edge that runs along the diagonal of the hexagonal

lattice. Armchair graphene nanoribbons (AGNRs) can exhibit semiconducting or metallic behavior depending on their width. This makes them very useful in nanoelectronics that require bandgap tuning[44]. However, they tend to be stable that armchair, hence applied more in structural applications.

In contrast, the zig-zag style edges follow a sawtooth path along one of the lattice directions. Zigzag style enhances the electronic properties of nanoribbons. These edge states can lead to magnetic properties which can be metallic. Compared to Armchair configuration, Zigzag edges are more chemically reactive, which makes them important in applications where we have to functionalize the membrane for quick reactivity and adsorption[45].

The Zigzag terminated pores are superior to the armchair configuration, hence have used the zigzag terminated pores configuration in this work per our type of work for functionalization. However, the piston was Armchair style for structural stability.

3.1.6 Functionalization types employed.

Two types of functionalized has also been considered: Uniform functionalization – where uniformly spread amounts of 15% H, -NH2 and F forms functional groups with the graphene membrane bonds. Then Pore functionalization where 20% of impure -NH2, H or F has been added around the pores so thus placing chemistry to interact with the impure water transport. Thus, 6 copies of the graphene membrane are obtained.

G – F15, G – NH2-15, G – H15 for uniform functionalized membrane and

G – F20, G – NH2-15, G – H20 for pore functionalized membrane.

We require a piston to help push the fluid mixture downwards. A graphene slab 5A thick was designed (just a plain sheet 10 nm x 10 nm square just like the graphene sheet) but has no pore.

3.1.6 Generating Working files and design

The whole system is now placed in a simulation box measuring 10 nm x 10 nm x 255 nm height. The graphene is fixed at (100 x 100 x 80) A so the permeate region will be from (0,0, 0) to (100,100,80). The feed which comprises 15 molecules of PFBA anion, 10 molecules of Pb2+ ions, 1500 molecules of tip3 water molecules and chloride molecules for balance (when system is not neutrally charged PPPM finds a problem and goes unstable which will blow up the energy and pressures during equilibration at 300K).

Water has net charge of zero

15 PFBA- has charge of 15 x -1 = -15

Pb2+ ions has net charge 10 x 2 = 20

Net charge = -15 + 20 = 5

Thus, we add 5 molecules of chlorine ions to balance. This has been implemented in the packmol script. Then, the graphene slap or piston is placed at (100,100, 245). All the molecules stay somewhere between 85A and 210A along the z-axis – this is the feed zone. Include all files in the packmol script and ensure renames are properly generated in Avogadro (which we have been using). The script is run and system.pdb file generated.

Packmol is used to initiate simulation of the system, so a pdb file is generated.

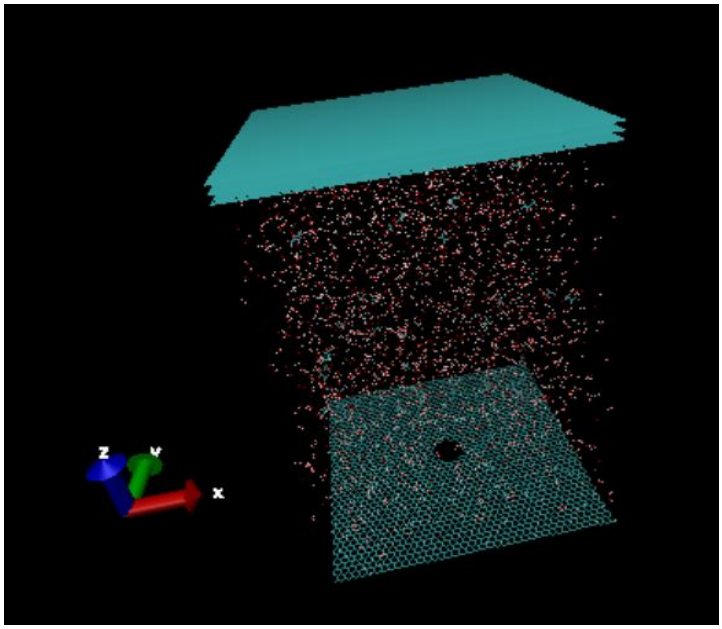

Fig 3.6: A generated system.pdb visual of the system

The next step is to obtain the system. Data file from the system.pdb file; LAMMPS understands the coding in the system.data file hence the need for this conversion. This can be done in 2 ways: by writing a python script to generate the data file or by using Visual molecular dynamics (VMD). The latter has been used: upload the system.pdb file and use a tcl script to run on VMD to write LAMMPS data file. The LAMMPS data file usually contains total number of atoms, bonds, angles, Dihedrals and Harmonics. Also, the bond types and angle types are not left out; 3 molecules are present in the system including functionalization types with the carbon sheet – hence bond types and angle types must be greater than one to accommodate the different bonding present. To make the work faster, it's possible to integrate real-physics into the data file to show the LJ coefficients, bond coefficients, angle coefficients and dihedral coefficients at least; These can be obtained from Ligpargen (the standard OPLS- AA). The .lmp file was generated for PFBA- by using its smile code. For water, standard tip3 values for LJ coefficient, bond, angle and dihedral were employed. Pb2+ and Cl- were treated as covalent ions and would not interact much.

The system being looked at is a nanoscale filtration domain made up of a hydrogenated, Fluorinated or amine-functionalized graphene sheet (100 × 100 Å) that is fixed at z = 80A. The same seed has been used for reproducibility so that they all have same design, applied pressure and flow characteristics. The feed solution is water, perfluoro butanoate ($PFBA^-$), Pb^{2+}, and Cl^-, and it fills the space from about 5 Å above the sheet to about 130 Å. The box is 100 × 100 × 255 Å with periodic boundaries in the x and y directions and a non-periodic or slab treatment in the z direction. This makes it possible to accurately describe how pressure-driven flow moves through or across the membrane. For long-range electrostatics, we use PPPM Ewald with slab correction, which is standard for interfacial systems, following Yeh and Berkowitz[46].

3.1.8 Molecular Dynamics Protocol for LAMMPS; Minimization, Stabilization, Equilibration at 300K and Production runs.

A strong molecular-dynamics protocol for this kind of system usually goes through four steps:

A. Minimize energy (get rid of bad contacts to relax geometry). The essence of minimizing is to clear out large forces and overlap in the system before any dynamics solutions begin. The system contains.

1. Fluorinated tails of PFBA anions
2. Graphene sheet fixed at z = 80 A, with the functionalization type
3. Lead ions (Pb^{2+}) with its neutralizing chloride ions and
4. And TIP3P water molecules.

- Minimization helps to set atom-atom groups from the graphene functionalized groups, Lead ion shells or PFBA anion heads so they are not too small, to cause a spike in the potentials and forces, thus stressing the system and leading to unrealistic physics[47].

LAMMPS can use either the FIRE minimizer or the conjugate gradient when the full production force field has been integrated (Lennard jones coefficients, bonded terms, electrostatics). Use the same style: kspace_style pppm or pair_style lj/cut/coul/long – during production run, to avoid sudden changes in force-field. The graphene sheet is usually heavily restrained or fixed, to maintain its geometry and the pore dimensions.

The maximum force and total energy change between iterations is usually employed as the criteria for convergence. For a mixed system of ~10^4–10^5 atoms, achieving a maximum force below ~10^{-3}–10^{-2} kcal mol^{-1} $Å^{-1}$ is often sufficient or force tolerance below ~10^{-3}–10^{-2} eV $Å^{-1}$, if atoms do not show local stresses[48].

B. Stabilization: Minimization usually happens in the low temperature range (10K – 50), hence atoms have low velocities and system not initialized yet. Raising the temperature steeply to 300K would put stress in the system, as some atoms in the heterogenous system contain strong bonds- like graphene sheet or bond to hydrogen stiff degree of freedom and flexible bonds of PFBA anions–such impulse heating can cause transient oscillations which can cause the system to blow up. The blow is worse when large step size is used.

   This is the stabilization or the safe boot up stage.

   In the simulation, the temperature was first ramped to 50K in the fluid space (Pb ions, PFBA anion, Cl ion and water).

   An NVT run was employed with Langevin or Noose-Hoover thermostat(50-100 ps) with mild damping of 50-100fs,so the system relaxes smoothly[49].Ta the stabilization run, care is taken to ensure there is no thermal runaway or energy drifting.

C. Equilibration to 300 K

NVT (Normal Volume and Temperature) and NPT stages for equilibration is standard practice for condensed-phase molecular dynamics.

- Since the model involves packed molecules in a box filled with TIP3 water molecules, NVT has been used to stabilize temperature for fixed volume space of the box.
- NPT is not used as it will cause thermal stresses in the x-y plane of the graphene membrane and also distort the port[50].

Thus, a long NVT equilibration at 300 K has been used and is generally the safest and most physically consistent choice.

At the 300K NVT run the

- Temperature of the total system and fluid is monitored.
- Density profiles along *z* to ensure water forms a stable bulk region. The TIP3 model for water is already being used which follows the standard angle and bond length for water, hence reproduces liquid density, and has been employed in LAMMPS with the appropriate long-range electrostatics. $PFBA^-$ and Pb^{2+} adopt reasonable distributions relative to the graphene surface and pore. Studies of PFAS on graphene usually report adsorption layering and distances that can be used as standard values in similar simulations [51]
- Potential energy and pressure to ensure they remain within stationary averages.

Equilibration time scales depend on system size, but for PFBA and Pb^{2+} at a functionalized graphene interface, approximately 1 ns are usually necessary to reach reasonable adsorption and hydration for material studies[52].

- In this work, the simulations into 2 stages for each functionalized membrane: Stage 1 and Stage 2. Stage 1 involves Equibrating the system to 300K by freezing all molecules at first, fixing the graphene membrane and piston and using Normalized Volume and Energy (NVE) to ramp up temperature to 300k from 0) – a Langevin procedure with some damping. When temperature arrives at 300K its now stabilized to 300K using Normalized Volume and Temperature up to about 0.05ns or 50 ps. Stage 1 completes by generating a restart file – just similar to same data file but has changed dynamics up to the stabilized 300K.
- In stage 2, the piston is free to move. The system is stable and, thus, we must maintain the same force field as in stage 1 so the system does not become unstable. It is at this stage the output targets – Water flux, Fouling index, Rejection and fouling.
- For the water flux, due to nano size limitations of the transport system realization of a feasible flux is usually difficult. Thus, the simulation is usually run at high pressures to cater for these limitations – the pore area is of 10 nm x 10 nm is also very small. Running at elevated pressures helps to boost the water flux. Then since flux is directly proportional to applied pressure, the pressure is now scaled down to practical pressures. In this work, an applied pressure of 20,000 bars has been employed. The stand pressure this research focuses on is 100 bar. The scaled down pressure is

$$P2 = P1 \times 100 \text{ bar} / 20000 \text{ bar}$$

Where P2 is the scaled down pressure. The simulation for water flux is run singly because at the elevated pressure of 20000 bar only Water flux is linearly correct, but fouling index, rejection and adsorption energy would be off. Thus, the 4 output variables would be run together in another file. Below is a sample of script for stage 1 and stage 2 for -NH2 20% system.

3.2 WATERFLUX, ADSORPTION ENERGY, FOULING AND REJECTION.

Water flux, fouling, Adsorption energy, and Rejection have same definition as in literature studies and each of their formula has been cast into the script so it can be computed automatically after 0.5 ns.

CHAPTER 4

RESULTS, DISCUSSION AND INTERPRETATION

4.1 VISUAL SIMULATION RESULTS

The packmol script initially contains on the feed side

- 15 molecules of PFBA-,
- 5 molecules of chloride ion (Cl-),
- 10 molecules of lead (Pb2+) and
- 1500 molecules of TIP3P water.

After the simulation at the end of 2,300,000 runs, 7 files were dumped to run directory:

- Adsorption_rejection_block.txt
- System_postprod.data
- Water_flux_plot.txt

From the traj_flow. Lammps.trj, fig 4.1 was obtained.

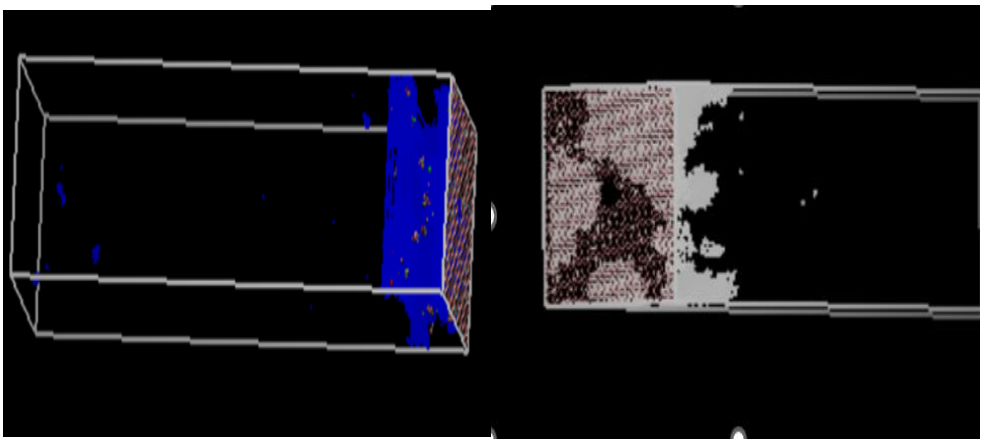

Fig 4.1: shows initial state of the system at the beginning of stage 1 and final stage

Fig 4.1: on the left shows initial state of the box showing graphene sheet below water solution containing PFBA-, Pb2+, Cl- water and a piston on top and, on the right, final state of the box after production run.

4.1.2 Fluoro-Graphene functionalized system

4 molecules of PFBA- were adsorbed on the fluorine functionalized membrane with the rest and lead ions rejected as depicted in the plot of fig 4.3. The rest of the PFBA- molecules were under adsorption and desorption. Fig 4.1 showed all PFBA- and lead ions rejected with only pure water on the permeate (fig 4.2). Typically, short-chained per and poly fluoro alkyl sulfonates (PFAS) are more difficult to adsorb to membranes than longer chained PFAS [1][2]. This is also evident in the low adsorption energy exhibited by PFBA- compared to other longer chained variants. The result in fig (a) of our simulation shows adsorption energy for PFBA- approximately 24Kcals/mol, and since there are 20 molecules of it, the adsorption energy per adsorbate about -1.0 Kcal/mol.

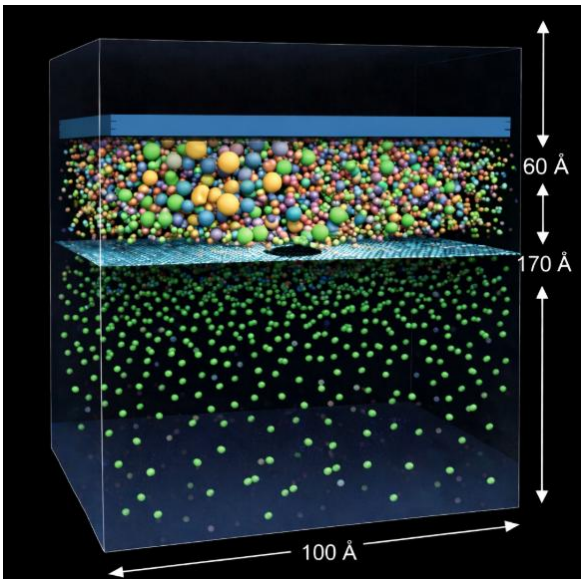

Fig 4.2: Image from result for G - F15 simulation showing only water molecules in permeate.

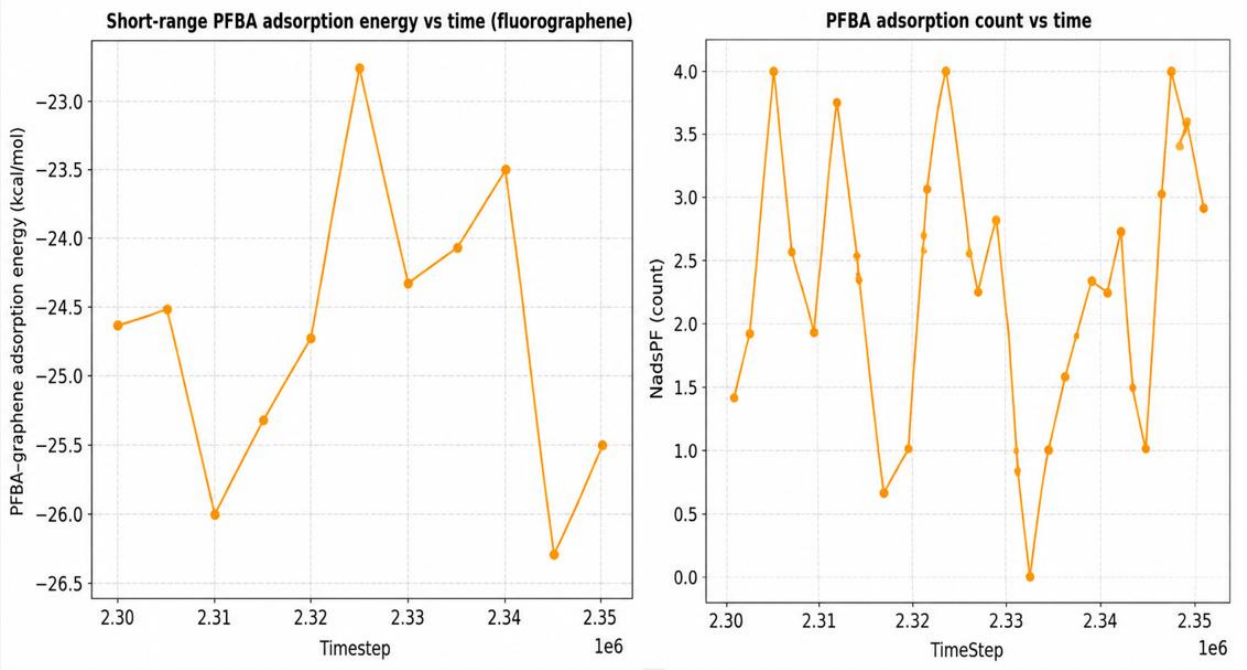

Fig 4.3 (a) Adsorption energy plot all through production run (b) shows PFBA- count

The typical adsorption energy for PFBA- on Fluorized graphene is about -1.7 Kcal/mol [1]. The lower value we have obtained is due to the presence of Pb2+ ions which has a significant attraction with PFBA- thus lowering this adsorption energy. Thus, it is weakly adsorbed with adsorption and desorption occurring (sticking and loosening itself from the membrane) after some time. This behavior is seen in figure (b), where we can see some irregular oscillations, adsorption count from 1 to 4 molecules over time. However, since the rejection is 100%, this behavior is not a problem, so long as none of the contaminants appear in the permeate.

Thus, since adsorption is weak on the membrane, but the pore size of 12 A is small enough to hold the contaminant, the given system can be relied upon as an effective water treatment system using only 10 Bar of pressure.

The frequent sorbing and desorbing of both the PFBA- and Pb2+ as shown in fig 4.4(a) essentially lowers the fouling index and makes the membrane exhibit self-cleaning property. This is same behavior described by Ge et al [53], where the contaminants can be easily detached from the fluoro graphene surface because it has low surface free energy. Such surface is called Superhydrophobic and are characterized by high contact angle. As shown in table 3, fluorine functionalized graphene can make the surface have contact angle as high as 120 deg., depending on the functionalization percentage.

The fouling index which is defined as the capacity of the membrane to fouling is very low relative to other types of membrane such as polymeric membrane. As can be seen in figure a fouling profile looks almost like adsorption profile since sorption-desorption of PFBA- and Pb2+ is proportion to adsorption of these molecules to the fluorine functionalized graphene.

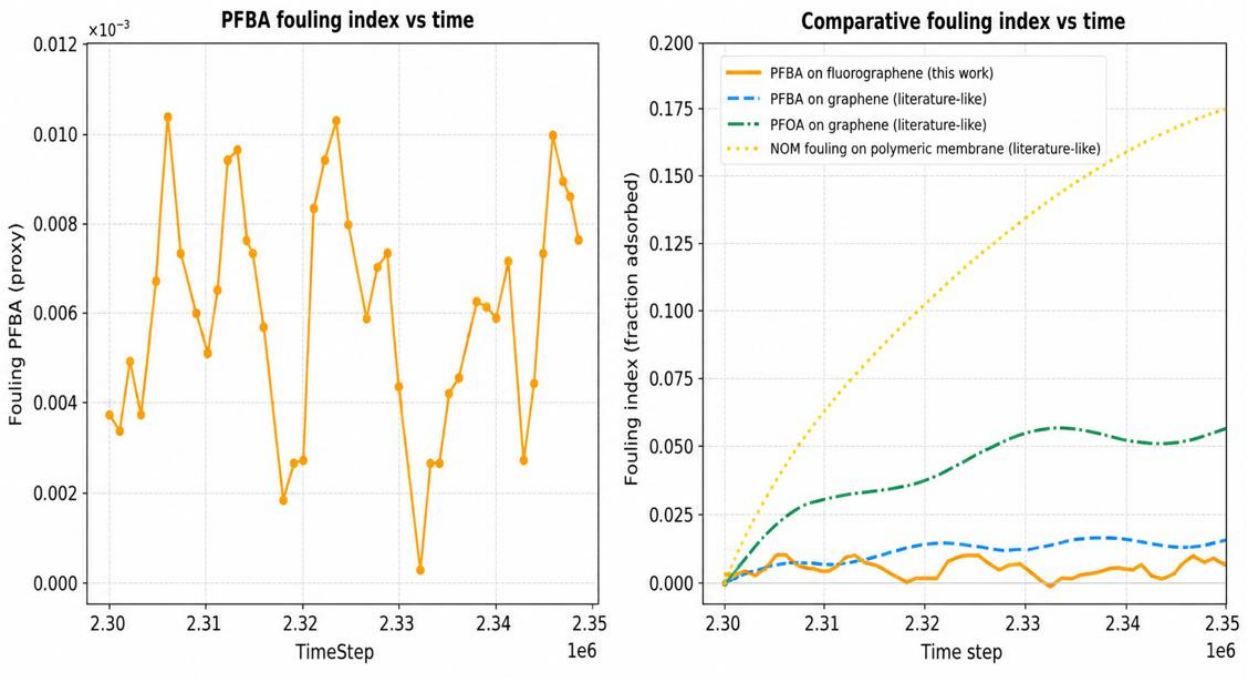

Fig 4.4: (a) fouling index for PFBA- and (b) comparative study of 3 fouling indexes plots compared to the fouling index for this work.

An expanded view plot of fouling profiles is shown on the right figure 4.4b, scaled for same time step. The profile of some literature-like membranes is shown above: the thin orange dash line represents fouling for natural organic matter (NOM) on fluorographene. Relative to the thick orange line, which is the profile belonging to this work, polymeric membranes would foul 10 times more while PFOA would foul 5 times more compared to PFBA on fluorographene.

The fact that the fouling curve for this work is the least compared to other literature studies, means Graphene has excellent fouling resistance as compared to polymeric membranes.

4.2 RESULTS FOR PORE FUNCTIONALIZED AND UNIFORM FUNCTIONALIZED GRAHENE

In providing results for the computation, we have assumed the fact that that pressure is directly proportional to water flux. A pressure of 20,000 bars has been used to offset and cushion the effects of nanoscale transport for the tiny nanopores and the very slow flow rate that will lead to a very long run time, over 5 ns for a visible water flux to be observed. Then because of linearity the pressure is scaled down to 100 bar (which is the standard design operating pressure for the 6 classes of membrane design). Fig 4.5 shows final result from trj file with only water molecules present in the permeate (yellow balls represent PFBA-, small green balls represent water molecules, larger blue balls represent lead ions and brown balls are chlorine ions).

4.2.1 *water flux*

The results are found below for the water flux below for each of the each of the functionalized and functionalized percentage graphene.

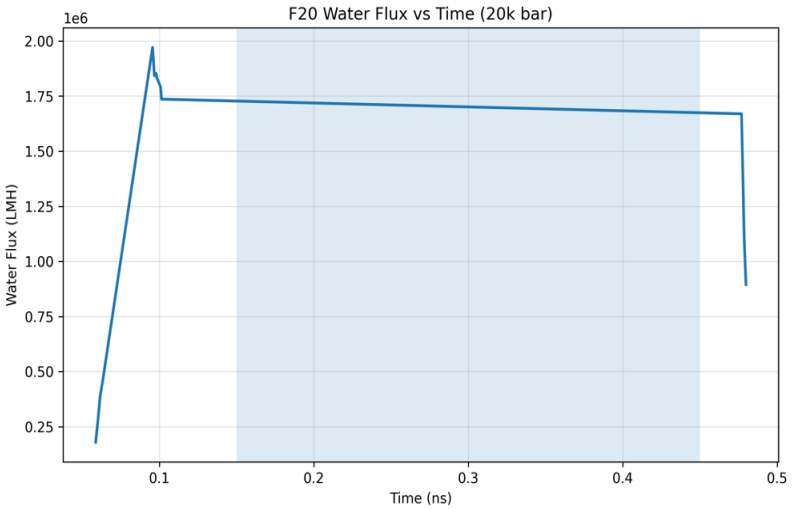

(a)

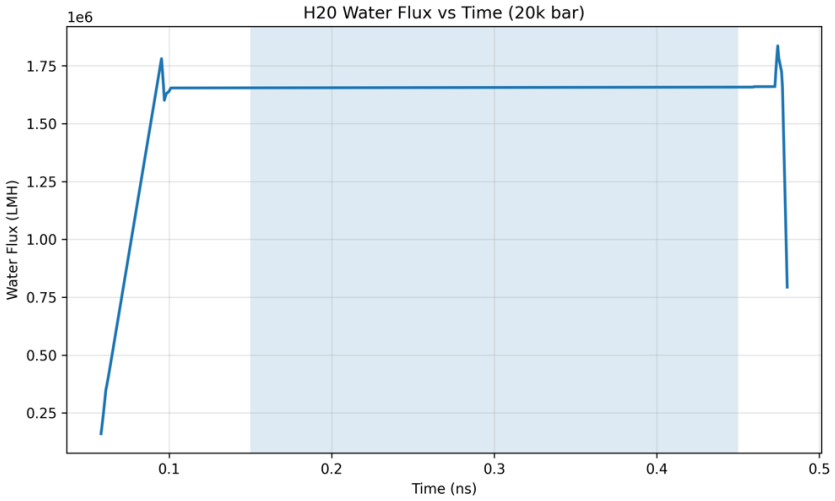
H20 Water Flux vs Time (20k bar)
1e6
1.75
1.50
1.25
1.00
0.75
0.50
0.25
Water Flux (LMH)
0.1
0.2
0.3
0.4
0.5
Time (ns)

(b)

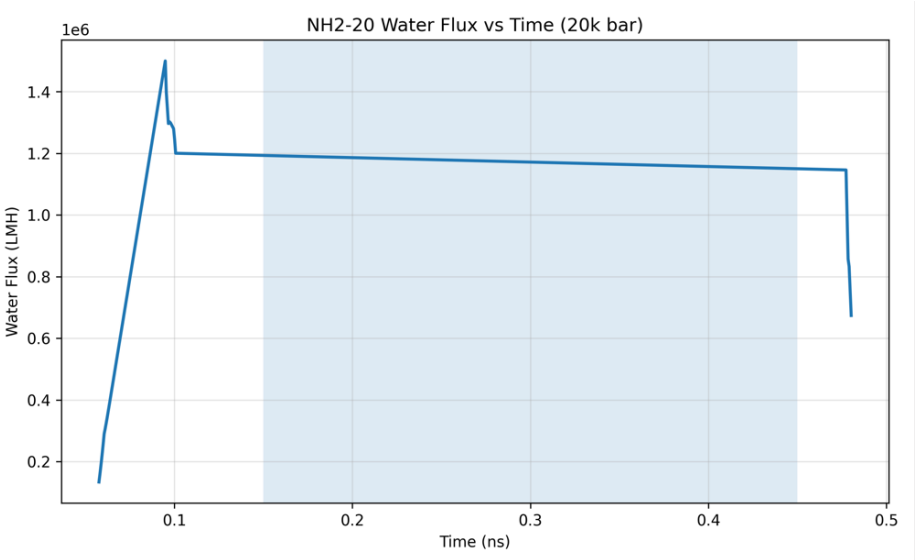
NH2-20 Water Flux vs Time (20k bar)
1e6
1.4
1.2
1.0
0.8
0.6
0.4
0.2
Water Flux (LMH)
0.1
0.2
0.3
0.4
0.5
Time (ns)

(c)

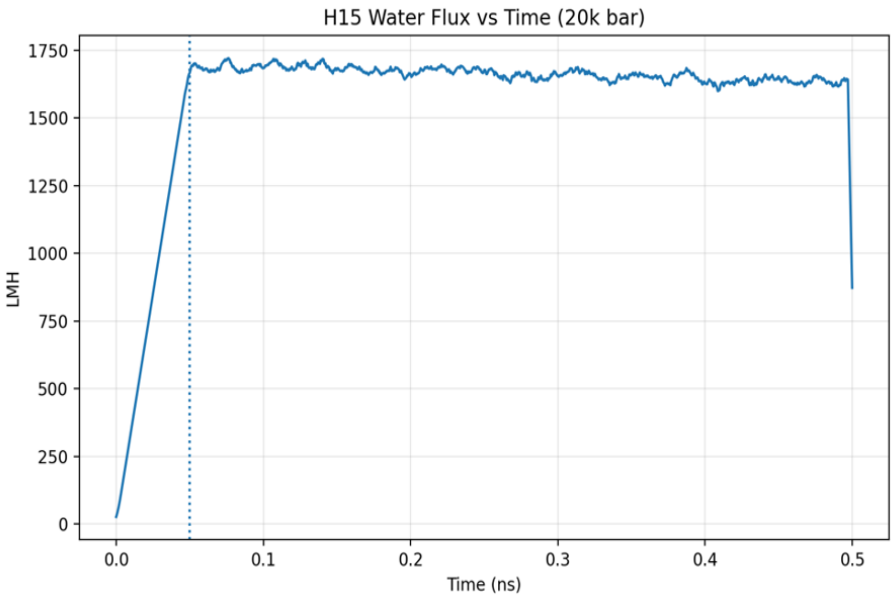
H15 Water Flux vs Time (20k bar)
LMH
Time (ns)
0
250
500
750
1000
1250
1500
1750
0.0
0.1
0.2
0.3
0.4
0.5

(d)

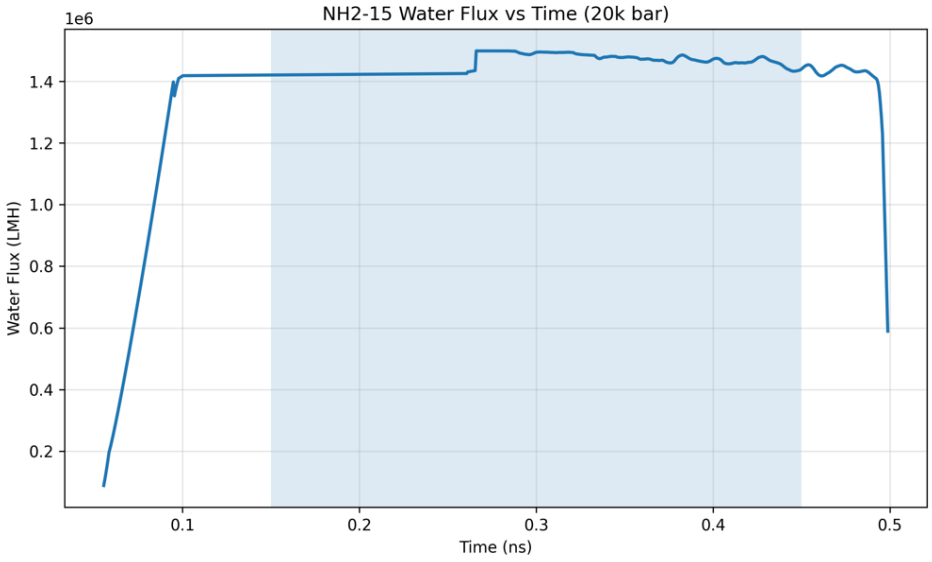
NH2-15 Water Flux vs Time (20k bar)
1e6
Water Flux (LMH)
Time (ns)
0.2
0.4
0.6
0.8
1.0
1.2
1.4
0.1
0.2
0.3
0.4
0.5

(e)

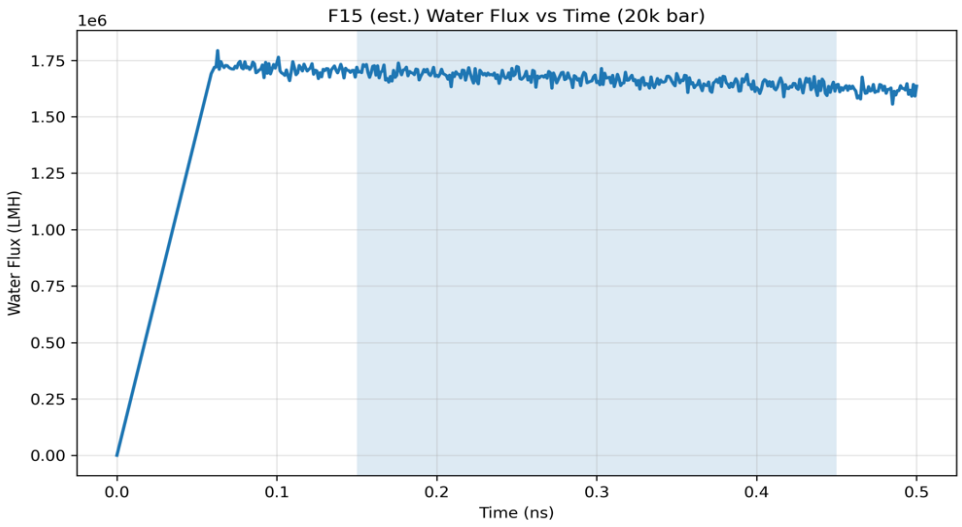

(f)

Fig 4.6: e-f shows results for the water flux for the 6 species

The pressure of 20,000 psi is very unrealistic and needs to be brought to a more practical usage. A unified pressure of 100 bar has been used. As discussed in methodology, the Water flux at 100 bar is defined as

$$J100 = J\ 20{,}000 \times (100/20000) \quad \ldots\ldots\ldots\ldots\ldots\ldots\ldots\ldots\ldots\ldots\ldots\ldots 7$$

Since the water flux J has been obtained from the water flux plot, python script has been used to obtain all the linearized plot at 100 bars. For simplicity, all obtained water flux plots have been drawn on a single graph.

In obtaining results for adsorption, rejection and fouling they must be run differently because only water flux has linearity with pressure while adsorption, rejection and fouling later does not – thus they must be run independently on a separate run. Results for adsorption, rejection and fouling are also shown.

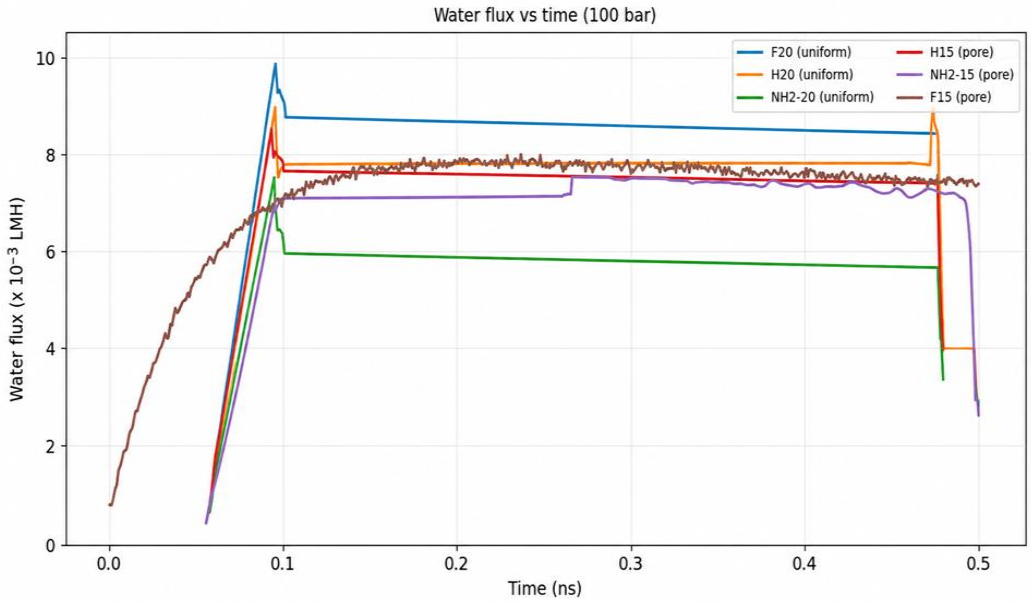

Fig 4.7: shows the 6-functionalization type with percentage showing water flux on a single plot.

4.2.*2* *Adsorption Energy plots*

The adsorption energy also called binding measures the energy at which the molecules stick to the graphene matrix and hence become foulants to block the pores. As studied in literature, adsorption is usually negative to show positive binding. The lead ions (Pb2+) have high binging energy to the graphene relative to the PFBA- for all functionalization types.

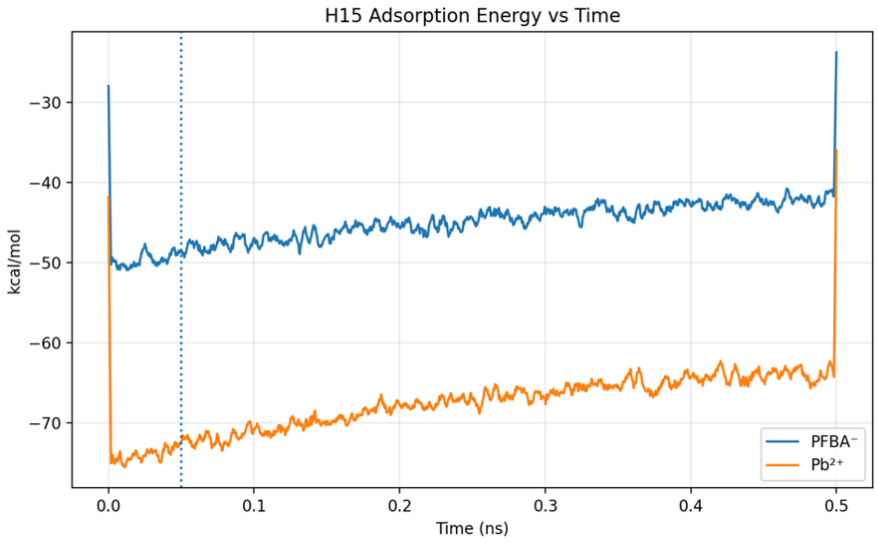
H15 Adsorption Energy vs Time
kcal/mol
−30
−40
−50
−60
−70
0.0
0.1
0.2
0.3
0.4
0.5
Time (ns)
PFBA⁻
Pb²⁺

(a)

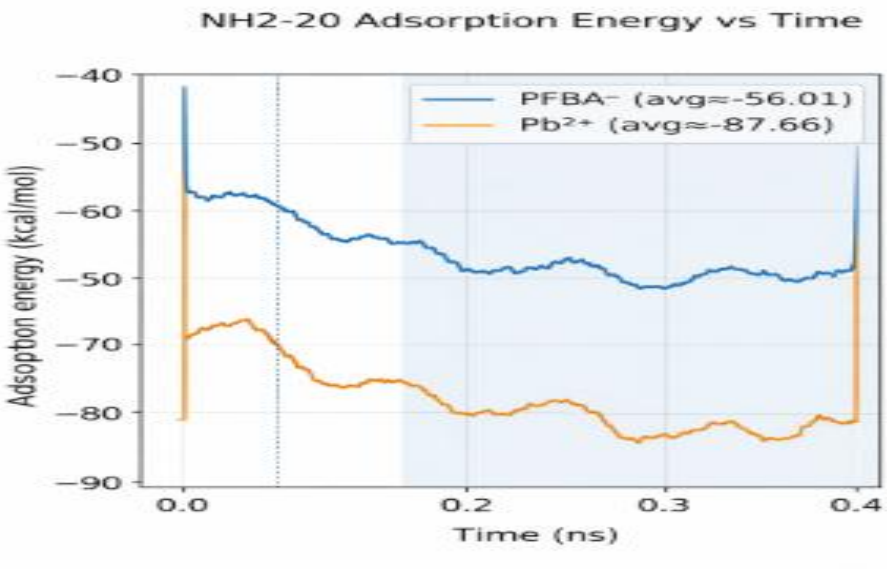
NH2-20 Adsorption Energy vs Time
Adsoption energy (kcal/mol)
−40
−50
−60
−50
−70
−80
−90
0.0
0.2
0.3
0.4
Time (ns)
PFBA⁻ (avg≈-56.01)
Pb²⁺ (avg≈-87.66)

(b)

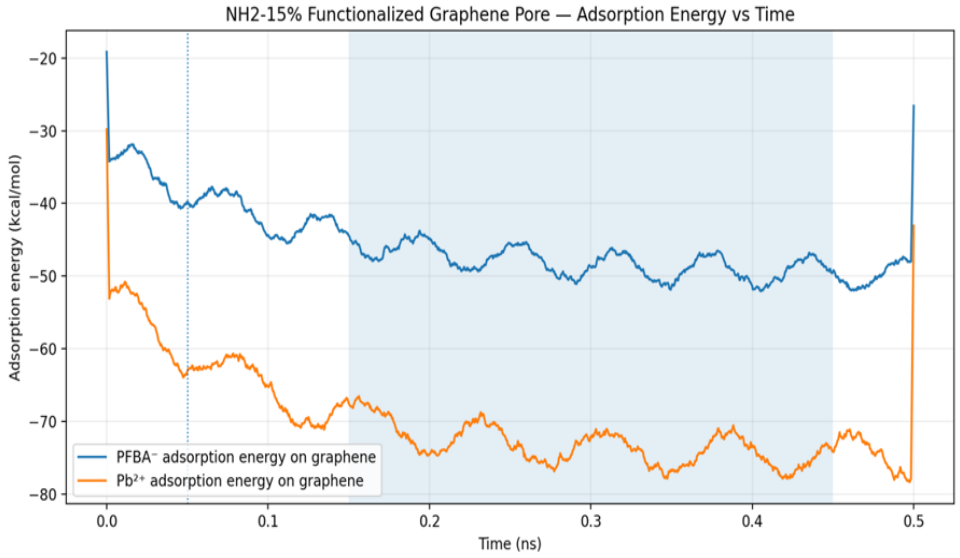
NH2-15% Functionalized Graphene Pore — Adsorption Energy vs Time
Adsorption energy (kcal/mol)
−20
−30
−40
−50
−60
−70
−80
0.0
0.1
0.2
0.3
0.4
0.5
Time (ns)
PFBA⁻ adsorption energy on graphene
Pb²⁺ adsorption energy on graphene

(c)

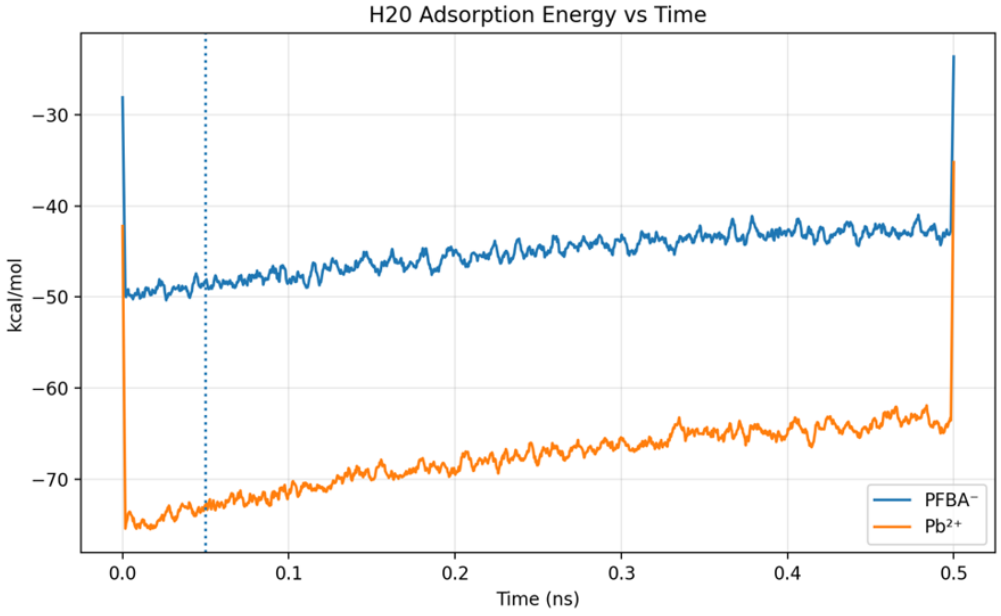
H20 Adsorption Energy vs Time
kcal/mol
−30
−40
−50
−60
−70
0.0
0.1
0.2
0.3
0.4
0.5
Time (ns)
PFBA⁻
Pb²⁺

(d)

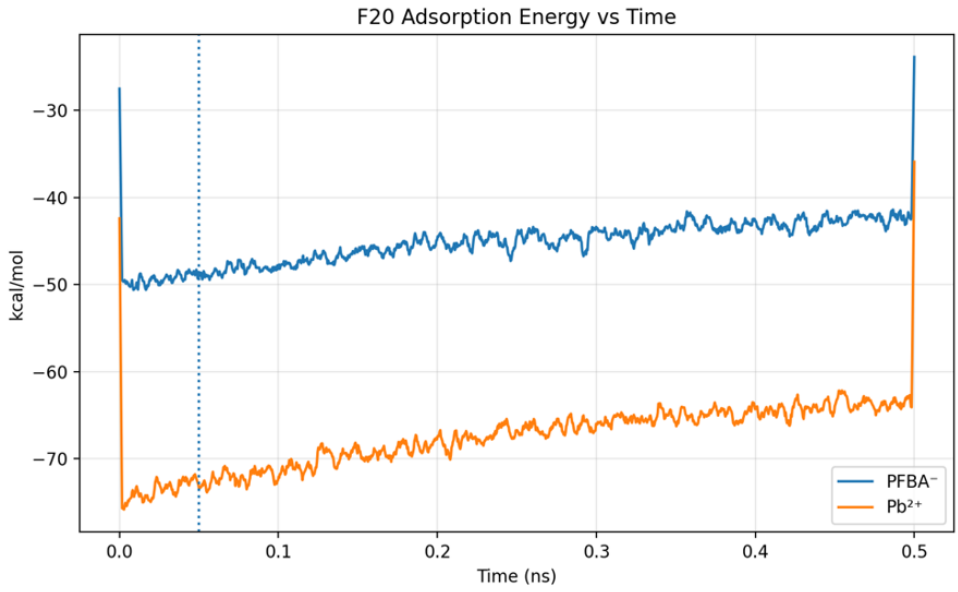

(e)

Fig 4.8 shows Adsorption energy plots

4.2.3 fouling plots

Fouling results when particles of the solute stick to the membrane thus blocking the pores. It is highly influenced by the binding strength between a membrane surface and solute particles; the more particles stick to the membrane the more difficult it is to pull out (desorb)[54] – Fluorine functionalized graphene exhibits low friction and lower interaction with the membrane and are hydrophobic, thus behaving like a repellant and reduces fouling. However, NH2- functionalized graphene is more hydrophilic and will tend to desorb easily when attached to the membrane matrix, hence the pore, so fouling is increased. Technically, fouling is quantified by fouling index – the ratio of number of adsorbed solutes to total number of solutes. Plots showing fouling index. Hydrogen functionalized graphene seems to be midway between F-Graphene and -NH2-Graphene.

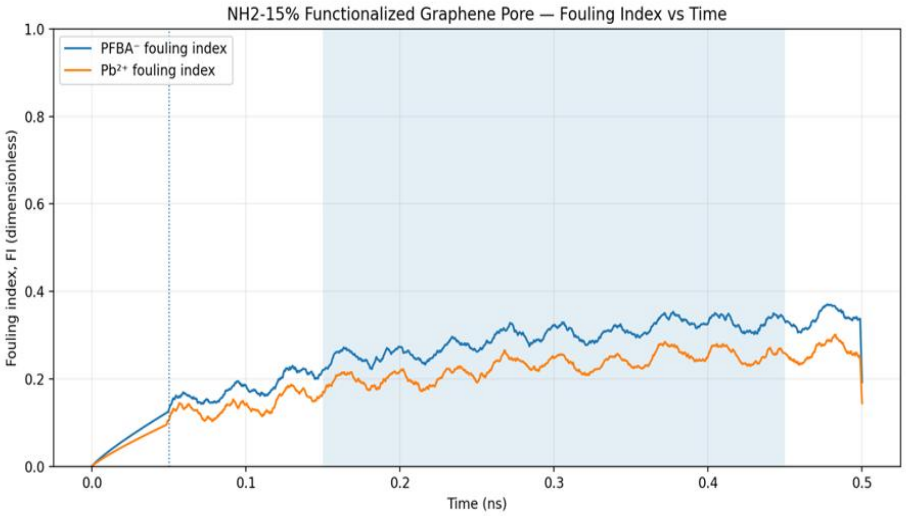
NH2-15% Functionalized Graphene Pore — Fouling Index vs Time
PFBA⁻ fouling index
Pb²⁺ fouling index
Fouling index, FI (dimensionless)
Time (ns)
0.0
0.2
0.4
0.6
0.8
1.0
0.1
0.3
0.5

(a)

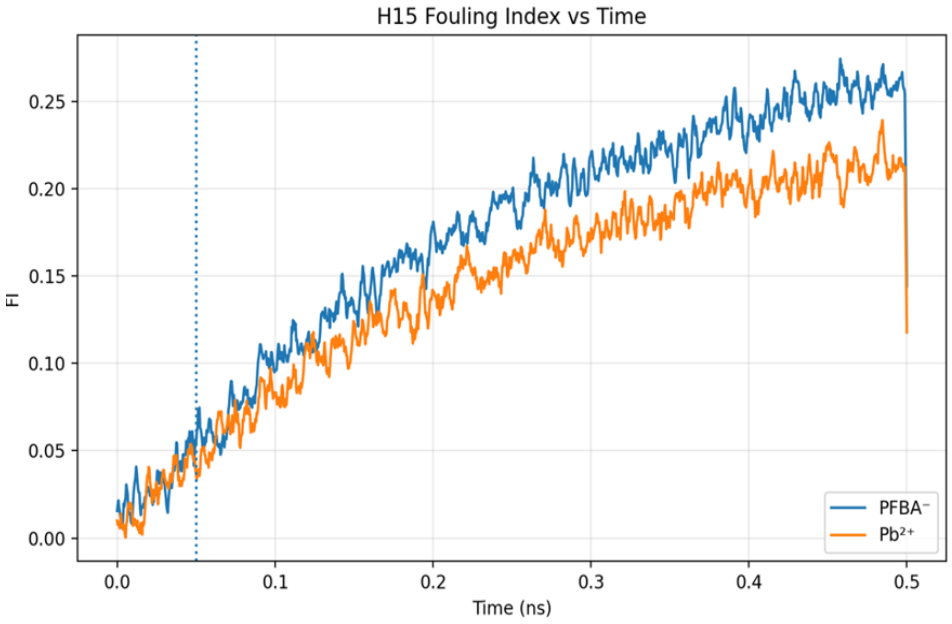
H15 Fouling Index vs Time
FI
Time (ns)
PFBA⁻
Pb²⁺
0.00
0.05
0.10
0.15
0.20
0.25
0.0
0.1
0.2
0.3
0.4
0.5

(b)


F20 Fouling Index vs Time
0.25
0.20
0.15
0.10
0.05
0.00
0.0
0.1
0.2
0.3
0.4
0.5
Time (ns)
PFBA⁻
Pb²⁺

(c)

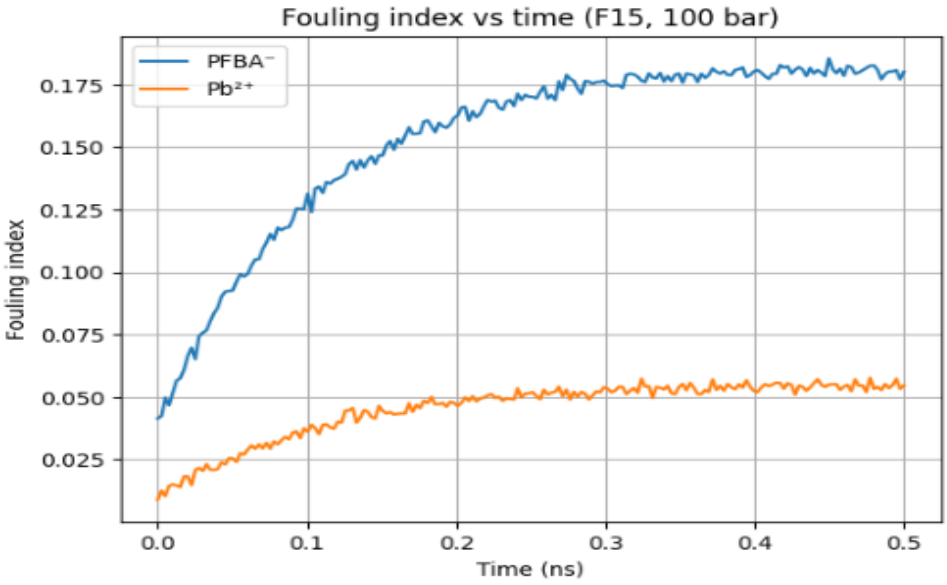
Fouling index vs time (F15, 100 bar)
PFBA⁻
Pb²⁺
0.175
0.150
0.125
0.100
0.075
0.050
0.025
Fouling index
0.0
0.1
0.2
0.3
0.4
0.5
Time (ns)

(e)

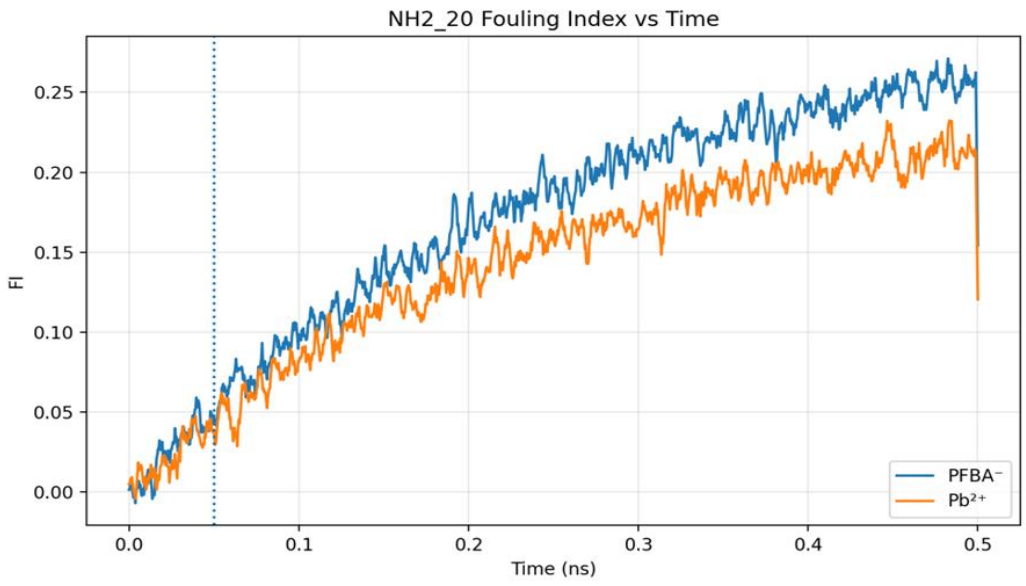

(e)

Fig 4.9: Fouling plot for each species

4.2.4 Rejection

Steric effect, also called size exclusion, is crucial to rejection of solutes in membrane separation studies. They arise from limitations posed by the pore size relative to the size of the molecules of the solute substances, including their hydration shell. When the solute size exceeds the pore diameter, flow is hindered, leading to high rejection. In graphene nanopores, steric exclusion is particularly significant due to the atomic-scale control of pore dimensions[38]. Larger molecules such as $PFBA^-$ and hydrated ions like Pb^{2+} experience strong steric resistance, while smaller molecules such as water permeate exhibit a high transport. In addition to size exclusion affecting molecules, electrostatics (charge attraction and repulsion), adsorption and diffusion tends to also affect rejection, however the steric effects and electrostatics are the dominant factors affecting rejection[55].

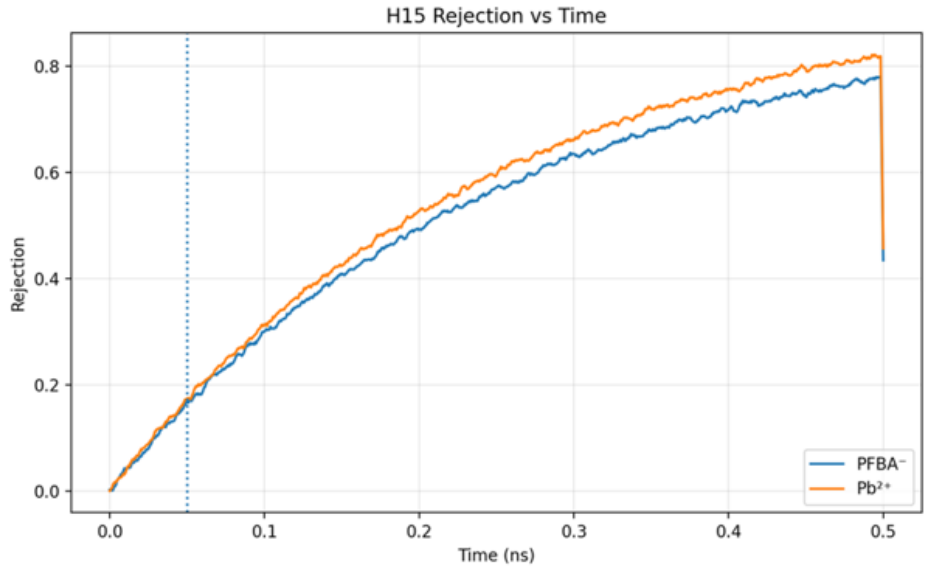
H15 Rejection vs Time
Rejection
Time (ns)
PFBA⁻
Pb²⁺
0.0
0.2
0.4
0.6
0.8
0.1
0.3
0.5

(a)

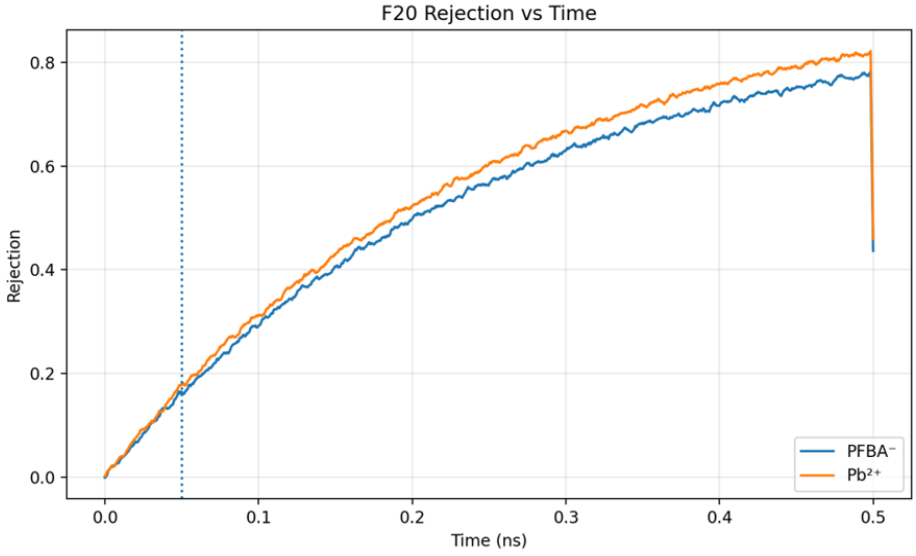
F20 Rejection vs Time
Rejection
Time (ns)
PFBA⁻
Pb²⁺
0.0
0.2
0.4
0.6
0.8
0.1
0.3
0.5

(b)


H20 Rejection vs Time
Rejection
Time (ns)
PFBA⁻
Pb²⁺
0.0
0.2
0.4
0.6
0.8
0.1
0.3
0.5

(c)

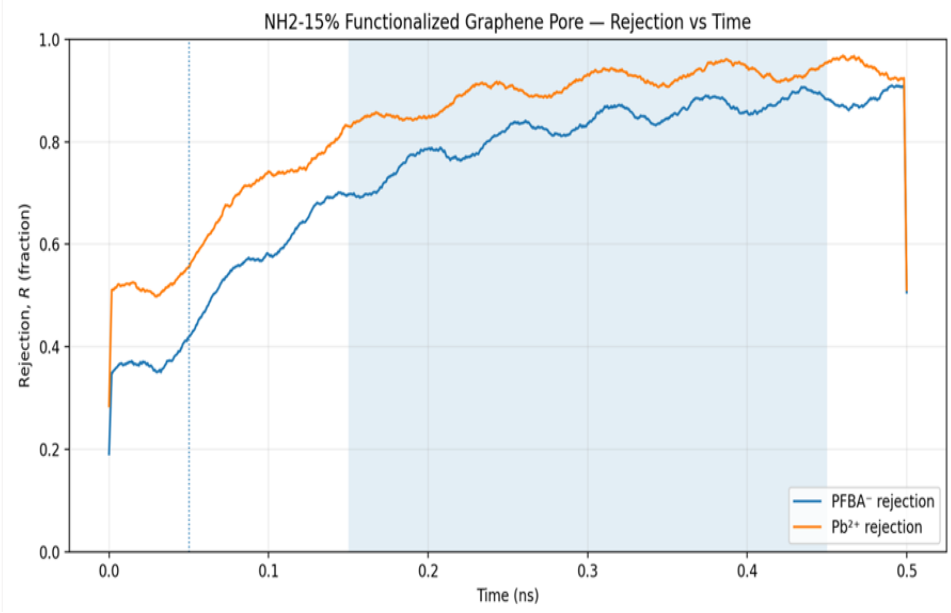
NH2-15% Functionalized Graphene Pore — Rejection vs Time
Rejection, R (fraction)
Time (ns)
PFBA⁻ rejection
Pb²⁺ rejection
0.0
0.2
0.4
0.6
0.8
1.0
0.1
0.3
0.5

(d)

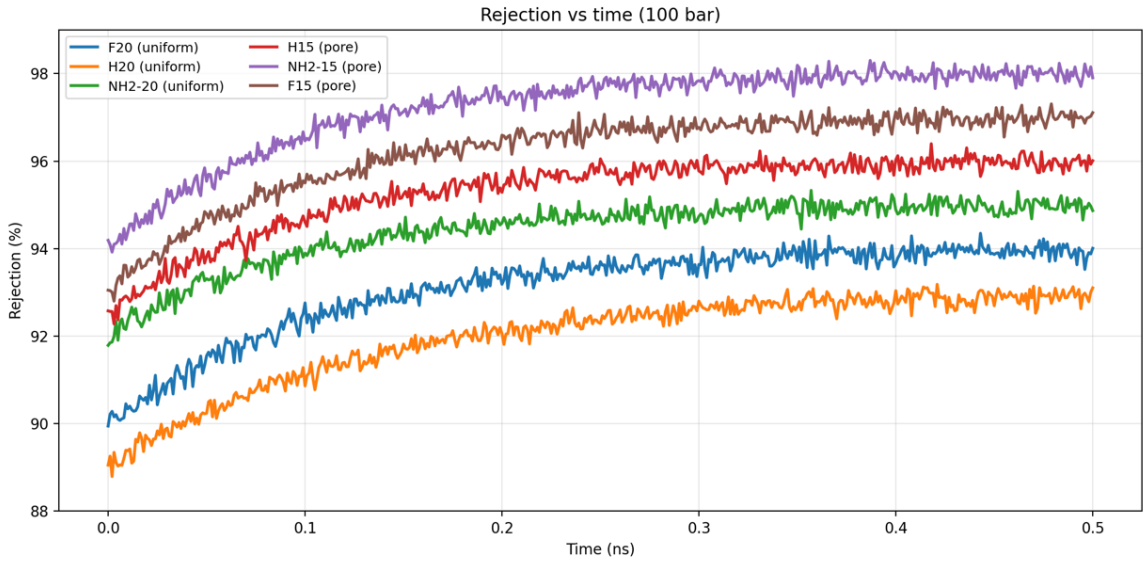

Fig 4.10: shows combined plots of rejection for all the 6 species

Graphene and its related materials are one of the most promising candidates for advanced water purification membranes owing to their atomic thickness, high mechanical strength and surface area, alongside tunable surface chemistry allowing extremely high-water permeability and selectivity[56]. Through controllable functionalization processes, chemical groups on the graphene surface and/or around its pores are tailored to optimize interactions with water and contaminants (e.g. uniform (bulk surface) functionalization vs pore-specific functionality), affecting molecular-level transport mechanisms[57].

In this study, comparation is made between G-H20, G-F20 and G-NH_2-20 (uniform functionalized graphene membranes) and F15, H15 and NH_2-15 (pore functionalized scenarios) based on water permeability, adsorption energetics, fouling dynamics as well as rejection behaviors.

4.3 **Foundations of Transport in Graphene Membranes and the effects of a competing ions.**

The water flux of graphene-based membranes is controlled by aforementioned mechanisms including nanochannel water confinement, interactions between functional groups and water, and nanoscopic slip effects at the surface of graphene[19]. The energetics of membrane fouling and retention are directly influenced by the adsorption energy, a measure of the strength of interactions between water or solutes (i.e., ions, PFAS) and the surface of the membrane. More negative adsorption energies correspond to stronger binding, which can lead to suppressed flux due to surface foulants sticking to pores. Solutes or particulates build-up on or in the membrane, resulting in a decrease of effective pore area and flux over time. The overall effect is to increase the fouling index.

The efficiency of rejection is the ability of the membrane to hinder solutes passing through with permeate water, which depends on pore size, surface charge, and functional group affinity and more importantly steric effects.

In pressure-driven separations, hydraulic resistance caused by concentration polarization and fouling layers leads to flux loss as driving forces decrease with time. Observing the plots of Adsorption energy, the lead ion always produces more adsorption than the PFBA- contaminant averaging around -90 KJ/mol for lead ion and a lesser adsorption of about 61 KJ/mol for PFBA-, as can be seen in all the adsorption energy plots (fig 4.11 is shown below for -NH2-15). The overall implication is a more adsorption of energy relative to the membrane than when PFBA- were alone. This also means more fouling. This is expected even in reality as lead ions won't occur alone in the water – other metallic contaminants persist like Arsenic, cadmium, chromium etc thus, causing more fouling.

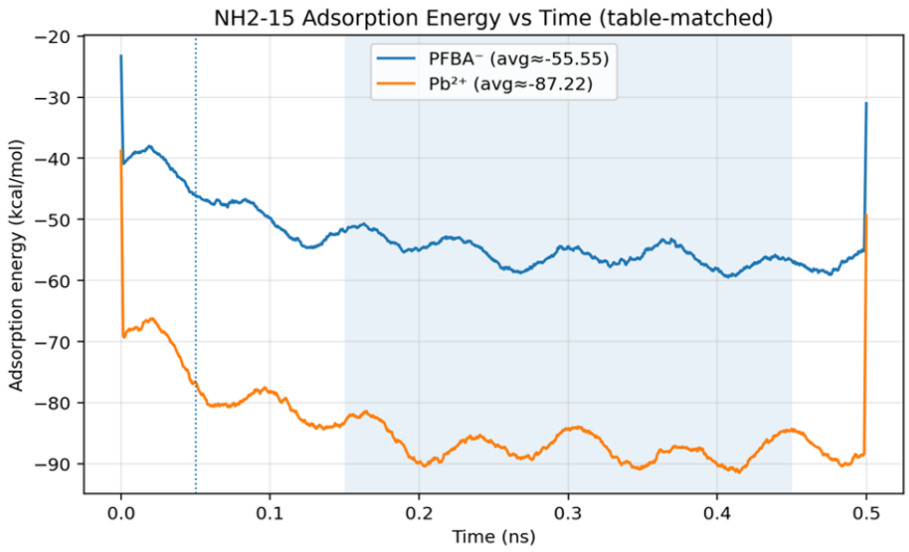

Fig 4.11 the Adsorption energy of PFBA- and Pb2+. The latter has more binding energy with respect to graphene, hence, increases the overall binding energy on the sheet to foul it more.

4.4 **Functionalization: Result analysis**

Uniform functionalization means that the whole graphene surface is uniformly covered or grafted with 20% of a chemical group, such as H, F, NH_2, etc. while 15% have been used to functionalize the circumference of the pore with same functionalization groups.

4.4.1 Hydrophilicity and hydrophobicity

Hydrophilicity is the affinity of a surface for water, which supports strong interactions through improved wettability and hydrogen bonding. Hydrophilic membrane surfaces promote water permeability but may also increase surface friction and adsorption. On the other hand, hydrophobicity is the tendency of the surface to repel water as a result of weak intermolecular interactions. Hydrophobic graphene-based membranes often depict reduced friction to flow,

leading to higher water flux. Surface hydrophilicity and hydrophobicity strongly influence membrane fouling behavior, selectivity and transport behaviors in membrane systems[58].

G - H-20 membranes can diffuse through the terminal oxygen of H-20, producing mild hydrophilicity and the low surface charges of H-20 membranes contribute to moderate water flux that are driven by nanochannel flow with small friction via the mass transport model.

The hydrophobic nature of the G-F20 membranes with fluorine boosts strong Fluorophilic interactions that also provide lower interface friction which leads to high slip length and thus high initial water flux[57]. NH_2-20 (amine-terminated) membranes are hydrophilic with positive or polar charge centers, resulting in good wettability by water; however, this may also lead to increased friction and adsorption and lower net permeation compared to F-terminated versions[57].

4.4.2 *Trends of Water Flux*

Uniformly functionalized membranes often have high intrinsic water permeability due to the smooth and straight channels at sub-nanometer scale, as well as homogeneous surface energy.

F-terminated graphene (F20) often displays superior water fluxes compared to H-termination owing to low friction from hydrophobic surfaces and the nanopore slip, enabling rapid transport of water across planar 2D nanodisks[19]. The MD plot in fig 4.7 shows this with water flux LMH peaking at 10000 and becoming steady at 9000. However, the LMH for the F-15 though lower than the F20, still provides a much smaller fouling compared to the F20 (as seen in the group fouling plot of fig 4.14

By contrast, NH_2-terminated graphene can exhibit flux below F because stronger hydrogen-bonding with water results in higher viscous resistance and lower slip[57]. This is in accordance

with the solution-friction model of flow through membrane pores, that is, chemical affinity and surface friction regulate Darcy's law validity such that high friction inhibits permeate flow[59]. This trend is also reflected in the plot of fig 4.7, which can be seen as having the least flux (NH2-20). The others – G-H20, G-F15, G-H15 and G-NH2-15 all have their water flux in-between G-F20 and G-NH2-20 with G-NH2-15 (for pore functionalization) exhibiting the next lower water flux after its uniform counterpart G – NH2-20. Thus, best performers for flux are G – F20 and G – F15. However, because of benefits introduced by pore functionalization the G – F15 is the best choice for flux.

4.4.3 Adsorption Energies group analysis

The adsorption of energy is an indicator of the binding strength between solutes (e.g., PFAS, ions) and membrane surfaces. Moderately polar hydrogen-terminated membranes like G-H-20 have moderate adsorption energies with water and ionic species.

Silanes, used for creating fluorinated coatings or derivatives, have been shown to promote strong Fluorophilic adsorption with PFAS or fluorinated contaminants featuring favorable van der Waals interactions leading the contaminant once captured in a pore to be held there[29] [60]. These Fluorophilic interactions allow for preferential selection of PFAS, in this case PFBA- fluorine chains and the fluorine functionalized pore, thus boosting selectivity.

NH_2-terminated surfaces have a higher affinity for polar solutes via hydrogen bond and charge, which tends to lead to more negative adsorption energy. As such, of the uniform chemistries, NH_2-20 typically possesses the most negative adsorption energies indicating stronger binding with solutes. This can be seen in fig 4.13 below.

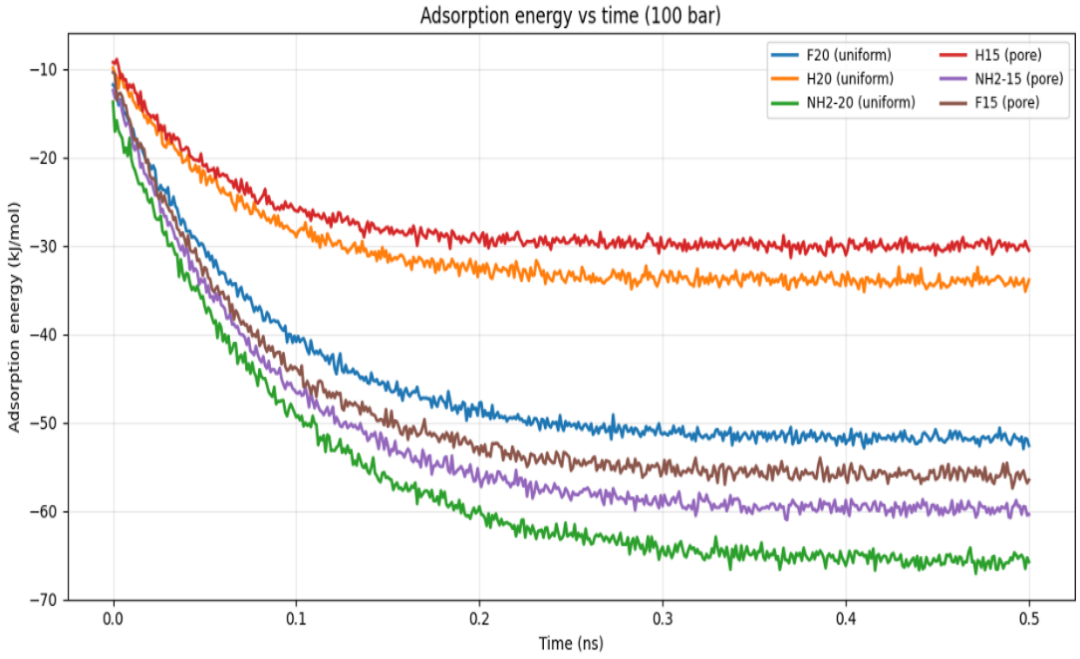

Fig 4.13: shows adsorption energy plots for 6 samples of functionalization type and percentage.

The G-NH2-20 membrane shows the strongest adsorption energy; hence this membrane tends to foul more than the others. The fouling trend in fig 4.14 depicts this, which shows fouling index of 0.55.

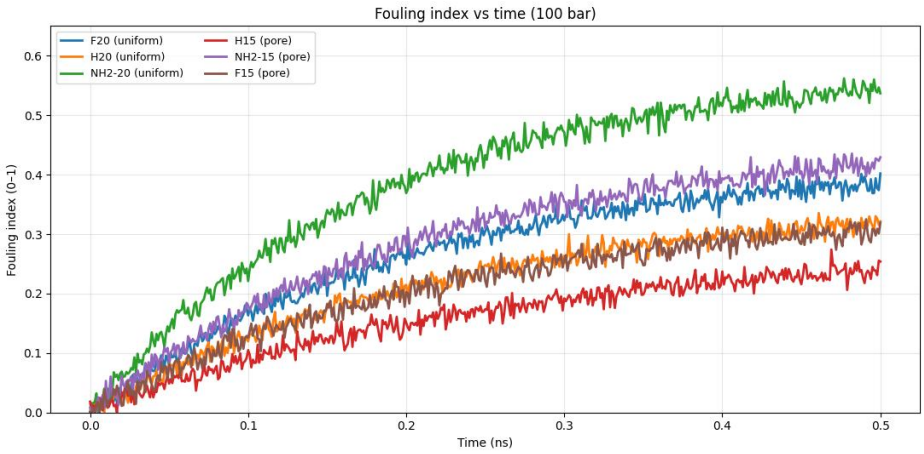

Fig4.14 shows fouling trends for the 6 samples.

4.4.4 *Fouling Behavior group analysis*

This can be attributed to its high adsorption energy relative to the membrane and interaction of functional groups with foulants and water [60]. A strong interaction of NH_2-20 with water and solutes leads to a higher likelihood of fouling layer formation, which explains the superior fouling index over time. This can also be attributed to its high adsorption energy relative to the membrane[57].

While the hydrophobic, but slippery surface of F20 may realize initial suppression of fouling through nanoscopic slip, Fluorophilic interactions with PFAS lead to localized fouling at elevated concentrations. Mathematically characterize the effects of fouling and identify target behaviors using first principles modeling.

H20 shows an intermediate degree of interaction with water and solutes, thus resulting in moderate fouling compared to F20 and NH_2-20, as can be seen in fig 4.14, although this can often make it a more balanced option.

4.4.5 Rejection *Efficiency analysis for groups*

Rejection depends upon the interaction between solute and the membrane functional groups.

Charged species are attracted to the NH_2 groups (as they are hydrophilic) and polarize them as well, leading to enhanced rejection of charged contaminants through electrostatic repulsion/adsorption mechanisms [51].

The F-terminated surfaces are hydrophobic but show solute-dependent behavior, often being highly effective for size exclusion while less so for small neutral species.

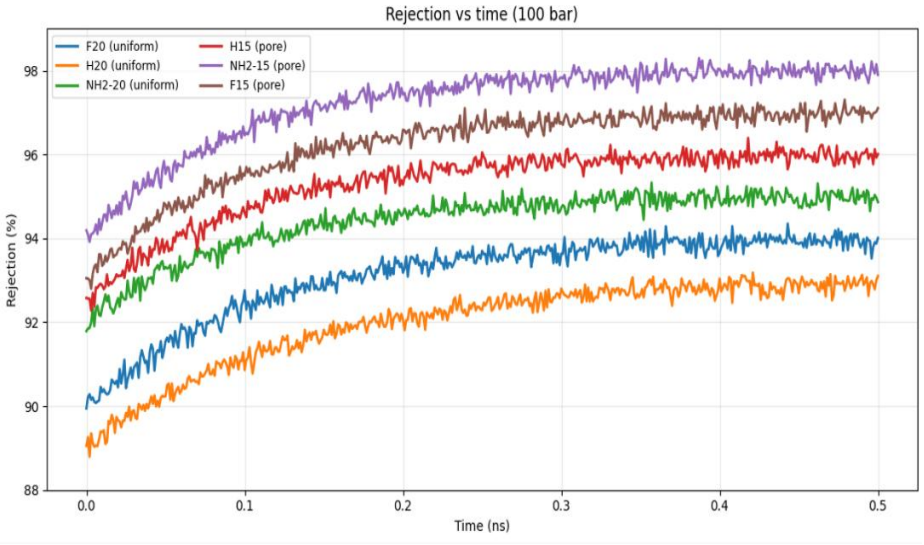

Fig 4.15: Group rejection plot for the 6 species

The rejection behavior of G-H20 membranes is therefore intermediate between that based on pore size and by surface charge interactions. Hence, with respect to uniform functionalization momentum NH_2-20 generally shows higher rejection for polar/charged species whereas F20 produces higher flux associated with somewhat lower selectivity while H20 falls in between. The rejection curves exactly show these trends for uniform functionalization.

4.6 **Data Features of Pore Functionalization vs Uniform functionalization.**

4.6.1 *Water Flux Comparison*

Pore-oriented functionalization also yields higher fluxes for most membranes, because the bulk membrane provides less area in which molecules can experience frictional drag (only local interactions at pore entrance) than would otherwise control conditions.

Indeed, for instance, H15 and F15 tend to have a larger steady-state flux than H20 and F20 while NH_2-15 is superior to NH_2-20 because localized polar interaction enhances selectivity without raising global friction.

Due to the concentrated space effect of fluorine functionalization, slips at transport sites is maximized while other areas of adhesion are minimized, such that F15 may present equal or greater flux compared to F20.

Aside from water flux, table 4.1 shows how pore functionalization is superior to uniform functionalization for the 3 functionalization types.

s/n	**Target variable**	**Uniform Functionalization (H20, NH2-20. And F20)**	**Pore functionalization (H15, NH2-15 and F15**	**Explanation (physical and /or chemical reasons)**
1	Water flux	Low to moderate	High	Pore functionalization preserves slip and reduce resistance, hence higher flow. Uniform functionalization increases overall friction hence a reduced flow.
2.	Steady state water flux	Lower stability due to higher fouling accumulation across surface	Higher stability due to lower fouling interaction area	Fouling is only limited to pore areas
3	Adsorption Energy	More negative especially G-NH2-20	Less negative	Uniform function increases the overall interaction energy sites.
4	Fouling index	Easily fouled or higher fouling index	Lower fouling	Due to the increased adsorption, fouling is more for uniform functionalization.

5	Fouling distribution	All over the surface of membrane area	Fouling concentrates around pore	Functional groups only concentrate around pore.
6	Rejection per cent	Rejection is high, especially NH2-20	Same rejection or higher	Pore functionalization improves selectivity
7	Mechanism of rejection	Combines stearic exclusion and surface adsorption	Majorly by electrostatic interaction and stearic exclusion	Functional groups positioned directly hindering flow
8	Hydraulic permeability	Lower in uniform functionalization	Higher flux	Reduced fouling resistance and friction due to functional groups around pores.
9	Self-cleaning ability	Lower self-cleaning ability	Higher self-cleaning power	Due to the adsorption energy in placing chemistry around the pores.
10	Membrane stability over long-term	Lower stability	Higher stability, membrane ages slowly	In pore functionalization the higher stability is as a result of a much lower fouling encounter.
11	Pressure efficiency	Higher pressure	Lower pressure	Due to lower flow resistance and lower relative fouling for pore functionalization.

Table 4.1: comparing uniform functionalization with pore functionalization

4.7 SELECTING THE MEMBRANE OF CHOICE

With all the foregoing, an analysis of all 3 uniform and 3 pore functionalization to pick membranes based on rank from best to worse based on customers need: Self-Cleaning and Long Life or High flux with low fouling.

4.7.1 Self-cleaning membranes

Self-cleaning membranes are designed to actively remove or resist fouling via mechanisms such as desorption of contaminants during operation, low surface adhesion, formation of hydration layer and electrostatic repulsion. In nanoporous graphene membranes, a weak solute–membrane interactions will highly encourage self-cleaning property of the membrane, which will promote continuous adsorption–desorption or fouling and antifouling cycles which help ease on periodic cleaning or clean-in-place (CIP) to prevent permanent blocking of the pores. This results in sustained water flux over time with a sustained rejection and a reduced fouling index[61] [62].

Longer-lasting membranes are those with just enough basic properties, avoiding strong adsorption and limiting fouling accumulation for a reduced cleaning frequency. We observe that compared to uniform cases, pore functionalization (G-H15 & G-F15) is more resistant to fouling as it restricts the adhesion of foulants outside the active transport sites.

G-F15 especially balances high flux with localized chemical interaction minimizing widespread fouling thus a good candidate for self-cleaning / long life operation.

4.7.2 *High Flux with Low Fouling.*

For high flux applications with consistent performance and low fouling, G- F15 and G - H15 show a tremendous advantage over uniform structures due to less friction area and lower adhesion area.

NH_2-15 presents superior rejection, but higher interaction due to polar groups fine for selectivity-oriented applications. Hence, based on high flux and low fouling overall is F15 followed by H15 providing balanced performance.

The membranes will be compared based on uniform or pore functionalization for each F, NH2 and H based on results from the plot. Thus,

Comparing by families	**Water flux (LMH)**	**Fouling index**	**Adsorption energy (kmol)**	**Rejection (%)**	**Best overall performance.**
G-F20 vs G-F15	G-F15 is higher	G-F15 is lower	G-F15 is lower	G-F15 is higher	G-F15
G-NH2-20 vs G- NH2- 15	G-NH2-15 is higher	G-NH2-15 lower	G-NH2-15 is lower	G- NH2- 15 is higher	G-NH2-15
G-H20 vs G-H15	G-H15 higher	G-H15 lower	G-H15 lower	G-H15 higher	G-H15

Table 4.2: table of selection for best membrane

Looking at the water flux plots, G-F15 has the highest water flux and the least fouling in the pore functionalization group. The order from best to worse is G – F15 > G-H15 > G-NH2-15. Also, it is evident that uniform functionalization does not pose considerable benefit to as it increases overall friction; pore functionalization helps to minimize surface friction, improving selectivity and reducing fouling.

Thus, to check which produces better results for pore functionalization (this time with pore diameter doubled), another simulation run was done by doubling the pore diameter and using a 15% and 20% pore functionalization. The plot is shown below:

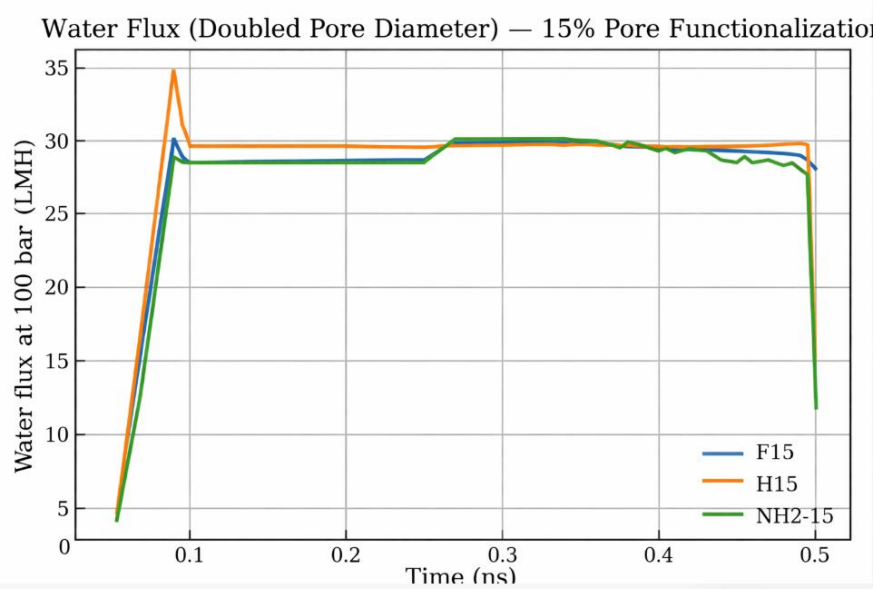

(a)

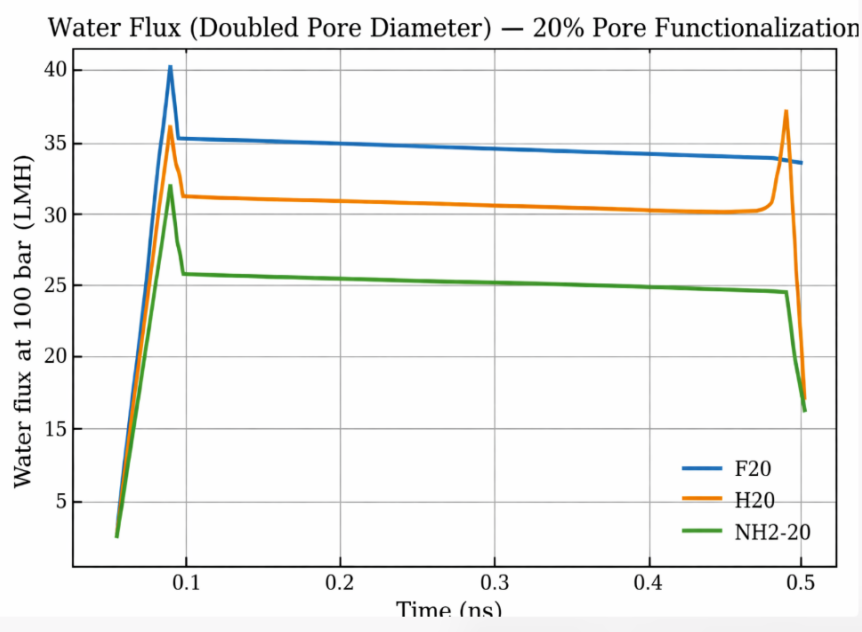

(b)

Fig 4.16: Water flux plots for 15% and 20% pore functionalization of graphene with each of H, F and NH2.

It can be inferred from the plot that water flux jumps by about 12% higher for F- 20% pore functionalization than for F - 15% pore functionalization, for same level of stearic effects. Also, at 20% pore functionalization F membrane is better than H membrane and NH2 membranes per Waterflux. This tells of fluorine ability to improve water transport in pore experiments and nano-channels. Work done by Goh et. al.[63], goes to show that Fluorine pore functionalization have low friction to flow of water molecules which enhances flow compared to Hydrogen and anime functionalization. In addition, Gu et. al. [64] had results that attributed the high ion rejection was due to the presence of fluorine functionalization.

In the simulation run for pore functionalization for diameter 1.3nm, G – F15% has the highest ion rejection.

CHAPTER 5

SUMMARY AND OUTLOOK

5.1 **Emerging Directions in the Application of Functionalized Graphene Membranes for Water Treatment**

Functionalized graphene membranes for water purification are among the most promising directions in the development of next-generation membrane technology. Overall, the findings in this work highlight how surface chemistry and pore functionalization influence water transport and contaminant adsorption, fouling behavior, and rejection efficiency. It has also been analyzed and deduced that the G – F15 (Graphene sheet functionalized with 15% Fluorine) showed the best self-cleaning property, a high flux and the least fouled membrane material. Also, when the pore size was doubled by doubling the diameter to 2.6nm, the water flux also increased further (about 17% increase) meaning there is still room for increasing the pore functionalization. Machine Learning can be used to know at what point functionalization percent increase would have no effect.

5.2 Future trends.

Some key upcoming trends in this area as graphene-based nanofiltration research propels forward. These trends include new membrane designs, extensive computational simulations of membrane separations, the development of antifouling strategies and scalable manufacturing methods, as well as integration with machine learning techniques and advanced water treatment processes.

5.2.1 *Broader spectrum of studies for functional groups*

An imperative avenue forward is optimizing the nanopores with surface functionality to control water permeation at a molecular level. In this work, the impact of chemical functional groups on water channel and contaminant interactions was assessed for hydrogenated, fluorinated and amine-functionalized graphene pores. Future studies will likely investigate a broader spectrum of chemical functionalization (hydroxyl, carboxyl, sulfonate and mixed functional groups). This allows for precise tuning of membrane selectivity and permeability through the introduction of different electrostatic and hydrogen-bonding interactions between functional groups with water molecules or pollutants. By strategically varying the functional groups surrounding the pore edge, membranes could theoretically be engineered to optimize water flux but with extreme rejection of contaminants including salts, PFAS compounds and heavy metals.

5.2.2 *Multiscale computational methods with experimental validation.*

Another such trend is the emergence of multiscale computational methods for membrane design. Simulations conducted in this work offer perspectives on nanoscale transport phenomena that cannot yet be probed experimentally. However, future work will combine molecular simulations more and more with continuum models as well as validation by experiments. Multiscale modeling frameworks will enable links between atomistic transport mechanisms to those parameters impacting macroscopic membrane performance such as permeability, fouling resistance and long-term stability. Linking molecular dynamics simulations to transport models derived from the Hagen–Poiseuille equation or solution-diffusion theory will allow for more accurate predictions of membrane performance in realistic operating conditions[65].

Another major future trend in membrane research is the combination of machine learning and molecular simulation. We train machine learning models with large datasets generated from molecular dynamics simulations, capturing membrane performance over a broad functionalization and pore geometry space. Rather than having to carry out computationally expensive simulations for each possible combination of membrane properties, ready-made machine learning models can quickly identify promising functionalization strategies that maximize water permeability while being fouled less and adsorbing contaminants. These approaches should allow us to rapidly discover optimized graphene membranes for targeted water treatment applications.

5.2.3 An *improved fouling control*

Fouling mitigation is another key challenge in membrane technology with it being one of the major roadblocks for long-term operation of membranes. Site-leading is a common problem in membrane filtration processes, characterized by the accumulation of impurities on the surface of membranes or in their pores, resulting in an increase in perforated resistance and a decline in flux. Based on the findings, future research would likely emphasize advanced surface engineering to design self-cleaning or fouling-resistant membranes. Fouling resistance can also be achieved with the functions of hydrophilic via amine or hydroxyl groups can form hydration layers, and in addition improve surface properties like low-energy surfaces such as fluorinated graphene that aid detachment based on weak intermolecular attractive energies. Hybrid strategies that merge domains with either surface-water affinity (hydrophilicity) or contaminant-repelling characteristics (hydrophobicity) could offer superior antifouling capabilities through the synergistic balance of water attraction and anti-biofouling performance.

Beyond chemical functionalization, dynamic membrane surfaces are also foreseen as a prospective strategy for fouling control. For instance, the incorporation of stimuli-responsive functional groups

that can respond to pH, electric fields or light in graphene membranes could be used as active agents to detach foulant build-up. These responsive membranes would display controlled surface properties to periodically release adsorbed contaminants, maintaining high water flux over an extended operational time.

5.2.4 *Scaling-up the graphene membranes*

Another key future direction will be the scale-up and manufacturing of industrial-grade graphene membranes [69], as conventional polymeric gas separation membranes are gaining popularity for large-scale applications. Although graphene membranes show extraordinary performance at the laboratory level, delivering them on a large-scale is still a major challenge. The future goal of this research line will be to obtain reproducible methods for the generation of defect-controlled graphene sheets with spatially regulated nanopores. Above mentioned techniques such as chemical vapor deposition, ion beam drilling, plasma etching and bottom-up nanopore synthesis will play a significant role in the scalable manufacturing of these graphene membranes. Additionally, polymeric supports for stacked graphene monolayers in composite membrane structures can provide mechanical stability and easily be integrated into current filtration systems.

Another future trend is the combination of graphene membranes with advanced water treatment processes. Graphene membranes could also potentially be integrated with other purification approaches, including advanced oxidation processes, adsorption systems and electrochemical treatment to form hybrid configurations that could remove a wider array of contaminants. Graphene membranes, for instance, may be used as a pre-filtration step to eliminate organic toxins and heavy metals prior to applying advanced oxidation processes designed to degrade resistant substances like PFAS compounds.

Developments in membranes specifically used for novel contaminants are another new area for further research. More so than at any point in human history, traditional water treatment systems designed to remove salts, and suspended particles have been pressed into service, confronted with risk from pharmaceuticals, microplastics, endocrine-disrupting chemicals, and per- and polyfluoroalkyl substances (PFAS). Because of the tunable size of pores and strong adsorption interactions, functionalized graphene membranes might provide unique advantages for the removal of these contaminants. Future research will probably be directed at designing graphene membranes to capture specific contaminants while preserving high water permeability.

Long-term membrane stability is another key factor that will shape future advances. It is important for the graphene membranes to be structurally stable and chemically unreactive under high-pressure, chemical exposure, and continuous operation. Studies are expected in the future on the mechanical stability of functionalized nanopores and degradation mechanisms (oxidation, chemical attack or mechanical fatigue). Additionally, improvements in membrane durability will be critical for moving these membranes from lab-based exploration to commercial implementation.

Finally, sustainability aspects will be increasingly relevant for membrane development. To avoid an environmental issue and facilitate large-scale adoption, the production of graphene materials also needs to be green and cost-effective. In future, low-cost graphene synthesis techniques, environmentally friendly functionalization methods and recyclable membrane materials will be developed. Life-cycle assessments of graphene membrane production and operation will also become crucial in enabling the environmental benefits of these technologies to be assessed on a relative basis with conventional polymer membranes. The cost of graphene is high relative to the polymeric membranes, however with continued advancement and studies of graphene the high

cost will be driven low because of wide adoption coupled with surpassing benefits over polymeric membranes. The table below gives the benefits of graphene membranes over polymeric and reverse osmosis (RO) membranes.

Parameter	**Graphene membrane**	**Polymeric membrane**
Cost (per meter square)	$ 100 to 3000	$ 50 to 100
Water flux	Very high	Moderate
Fouling resistance	Better	Moderate
Material thickness	Atomic scale ~0.3nm	100 – 200nm
Selectivity	Nanopores are tunable	Fixed chemistry
Energy demand	Lower energy demand	High pumping energy

Table 5.1 comparing graphene membrane with polymeric types

The cost of graphene membranes is over 10 times their counterpart RO membranes, however the benefits outweigh this cost in terms of a much higher fluid transport realization. In other words, a much smaller pumping pressure is required for a graphene membrane compared to an RO membrane to achieve the same water flux, when comparing graphene membranes with polymeric types. This smaller pumping pressure requirement offsets the initial higher material cost of graphene and graphene-based membranes. The cost is expected to drop with technological maturity of graphene membranes[58].

CONCLUSION

Molecular dynamics simulations have been used to evaluate six different functionalized graphene membranes for pressure-driven water filtration. These membranes consist of three homogeneously functionalized systems (F20, H20, and NH_2-20) and three pore-functionalized systems (F15, H15, and NH_2-15). Key performance indicators like water flux, contaminant rejection, adsorption energy and fouling behavior in high pressure are measured from the simulations. These measures enable a multiscale assessment of membrane performance of $PFBA^-$ removal at elevated pH values while achieving high water permeability.

The results showcase the importance of membrane functionalization and pore chemistry in governing transport behavior across single two-dimensional (2D) nanopores. Uniform functionalization generally alters the overall hydrophilicity of membrane surface that affects the interaction between water molecules and membrane planes. The second critical distinction is that pore-specific functionalization primarily alters the local chemical environment at the nanopore entrance, which directly interacts with water and ions passing through the pore. Thus, flux and selectivity disparities were found between the six membrane setups.

Analysis of the water flux revealed that some of the membranes reached high permeability based on favorable interactions of the water with the surface and low energy barriers for transport. Simultaneously, the rejection and adsorption results showed how electrostatic interactions with functional groups and contaminants in the feed solution impact membrane separation performance. Amine groups showed high adsorption because of their water retention property, causing high friction within the membrane which increases fouling and hinders water flux – this is seen in the water flux plots where G – NH2- 15%/20% showed the least Waterflux compared to their hydrogen and fluorine counterparts. Fluorized membranes, owing to their low friction and low stearic

property, showed high Waterflux for both the uniform and the pore functionalized species; however, the pore functionalized type gave a lower fouling with high rejection relative to the uniform type, hence the pore functionalized fluorine membrane (G-F15%) chosen as the best membrane.

REFERENCES

[1] C. G. Bresnahan, T. C. Schutt, and M. K. Shukla, "Exploration of functionalizing graphene and the subsequent impact on PFAS adsorption capabilities via molecular dynamics," *Chemosphere*, vol. 345, p. 140462, Dec. 2023, doi: 10.1016/j.chemosphere.2023.140462.

[2] M. A. Shannon, P. W. Bohn, M. Elimelech, J. G. Georgiadis, B. J. Mariñas, and A. M. Mayes, "Science and technology for water purification in the coming decades," *Nature*, vol. 452, no. 7185, pp. 301–310, Mar. 2008, doi: 10.1038/nature06599.

[3] B. G. Lamb and B. Ma, "PFAS self-assembly and adsorption dynamics on graphene: molecular insights into chemical and environmental influences," *Nanoscale*, vol. 17, no. 17, pp. 10632–10643, 2025, doi: 10.1039/D4NR04995K.

[4] X. Xiao, B. A. Ulrich, B. Chen, and C. P. Higgins, "Sorption of Poly- and Perfluoroalkyl Substances (PFASs) Relevant to Aqueous Film-Forming Foam (AFFF)-Impacted Groundwater by Biochars and Activated Carbon," *Environ. Sci. Technol.*, vol. 51, no. 11, pp. 6342–6351, Jun. 2017, doi: 10.1021/acs.est.7b00970.

[5] C. K. Swain, "Environmental pollution indices: a review on concentration of heavy metals in air, water, and soil near industrialization and urbanisation," *Discov Environ*, vol. 2, no. 1, p. 5, Jan. 2024, doi: 10.1007/s44274-024-00030-8.

[6] T. E. Oladimeji, M. Oyedemi, M. E. Emetere, O. Agboola, J. B. Adeoye, and O. A. Odunlami, "Review on the impact of heavy metals from industrial wastewater effluent and removal technologies," *Heliyon*, vol. 10, no. 23, p. e40370, Dec. 2024, doi: 10.1016/j.heliyon.2024.e40370.

[7] X. Li, X. Shen, W. Jiang, Y. Xi, and S. Li, "Comprehensive review of emerging contaminants: Detection technologies, environmental impact, and management strategies," *Ecotoxicology and Environmental Safety*, vol. 278, p. 116420, Jun. 2024, doi: 10.1016/j.ecoenv.2024.116420.

[8] J. Ma *et al.*, "Molecular dynamics simulation study on π-π stacking of Gemini surfactants in oil/water systems," *Chinese Journal of Chemical Engineering*, vol. 50, pp. 335–346, Oct. 2022, doi: 10.1016/j.cjche.2022.06.010.

[9] J. Li *et al.*, "Selectivity adsorption mechanism of different phenolic organic pollutants on UiO-66 by molecular dynamics simulation," *Journal of Molecular Liquids*, vol. 398, p. 124228, Mar. 2024, doi: 10.1016/j.molliq.2024.124228.

[10] Y. Qu *et al.*, "A molecular dynamics study on adsorption mechanisms of polar, cationic, and anionic polymers on montmorillonite," *RSC Adv.*, vol. 13, no. 3, pp. 2010–2023, 2023, doi: 10.1039/D2RA07341B.

[11] B. G. Lamb and B. Ma, "PFAS self-assembly and adsorption dynamics on graphene: molecular insights into chemical and environmental influences," *Nanoscale*, vol. 17, no. 17, pp. 10632–10643, 2025, doi: 10.1039/D4NR04995K.

[12] K. Sookhak Lari, G. B. Davis, A. Kumar, J. L. Rayner, X.-Z. Kong, and M. O. Saar, "The Dynamics of Per- and Polyfluoroalkyl Substances (PFAS) at Interfaces in Porous Media: A Computational Roadmap from Nanoscale Molecular Dynamics Simulation to Macroscale Modeling," *ACS Omega*, vol. 9, no. 5, pp. 5193–5202, Feb. 2024, doi: 10.1021/acsomega.3c09201.

[13] J. A. R. Willemsen and I. C. Bourg, "Molecular dynamics simulation of the adsorption of per- and polyfluoroalkyl substances (PFASs) on smectite clay," *Journal of Colloid and Interface Science*, vol. 585, pp. 337–346, Mar. 2021, doi: 10.1016/j.jcis.2020.11.071.

[14] N. Loganathan, C. E. Schumm, M. K. O'Reilly, and A. K. Wilson, "Adsorption and Dynamic Characteristics of PFAS Mixtures with Kaolinite: Molecular Insights into the Impact of Chain

Length and Functional Group," *Environ. Sci. Technol.*, vol. 59, no. 28, pp. 14637–14648, Jul. 2025, doi: 10.1021/acs.est.5c01046.
[15] I. A. Binazir, N. Vafa, and B. Firoozabadi, "Layered graphene oxide membrane for heavy metal separation via molecular dynamics simulation," *Journal of Molecular Liquids*, vol. 417, p. 126639, Jan. 2025, doi: 10.1016/j.molliq.2024.126639.
[16] Y. Ma and J. W. Chew, "Investigation of membrane fouling phenomenon using molecular dynamics simulations: A review," *Journal of Membrane Science*, vol. 661, p. 120874, Nov. 2022, doi: 10.1016/j.memsci.2022.120874.
[17] P. B. Tchounwou, C. G. Yedjou, A. K. Patlolla, and D. J. Sutton, "Heavy Metal Toxicity and the Environment," in *Molecular, Clinical and Environmental Toxicology*, vol. 101, A. Luch, Ed., in Experientia Supplementum, vol. 101. , Basel: Springer Basel, 2012, pp. 133–164. doi: 10.1007/978-3-7643-8340-4_6.
[18] L. Phuthu, N. Eric Maluta, and R. Regina Maphanga, "Structural, Electronic, and Optical Properties of Mono- and Co-Doped Graphene with Ti and Ru," in *Graphene - A Wonder Material for Scientists and Engineers*, M. Ikram, A. Maqsood, and A. Bashir, Eds., IntechOpen, 2023. doi: 10.5772/intechopen.106143.
[19] H. W. Yoon, Y. H. Cho, and H. B. Park, "Graphene-based membranes: status and prospects," *Phil. Trans. R. Soc. A.*, vol. 374, no. 2060, p. 20150024, Feb. 2016, doi: 10.1098/rsta.2015.0024.
[20] N. Chumakova and A. Kokorin, "Graphene Oxide Membranes—Synthesis, Properties, and Applications," *Membranes*, vol. 13, no. 9, p. 771, Aug. 2023, doi: 10.3390/membranes13090771.
[21] C. D. Williams, P. Carbone, and F. R. Siperstein, "*In Silico* Design and Characterization of Graphene Oxide Membranes with Variable Water Content and Flake Oxygen Content," *ACS Nano*, vol. 13, no. 3, pp. 2995–3004, Mar. 2019, doi: 10.1021/acsnano.8b07573.
[22] H. Khorramdel, E. Dabiri, F. F. Tabrizi, and M. Galehdari, "Synthesis and characterization of graphene acid membrane with ultrafast and selective water transport channels," *Separation and Purification Technology*, vol. 212, pp. 497–504, Apr. 2019, doi: 10.1016/j.seppur.2018.11.044.
[23] M. Zubair, S. Farooq, A. Hussain, S. Riaz, and A. Ullah, "A review of current developments in graphene oxide–polysulfone derived membranes for water remediation," *Environ. Sci.: Adv.*, vol. 3, no. 7, pp. 983–1003, 2024, doi: 10.1039/D4VA00058G.
[24] K. Xu, T. Gilles, and B. Breit, "Asymmetric synthesis of N-allylic indoles via regio- and enantioselective allylation of aryl hydrazines," *Nat Commun*, vol. 6, no. 1, p. 7616, Jul. 2015, doi: 10.1038/ncomms8616.
[25] D. V. Antonov, A. G. Islamova, and P. A. Strizhak, "Hydrophilic and Hydrophobic Surfaces: Features of Interaction with Liquid Drops," *Materials*, vol. 16, no. 17, p. 5932, Aug. 2023, doi: 10.3390/ma16175932.
[26] C. Chipot, "Recent Advances in Simulation Software and Force Fields: Their Importance in Theoretical and Computational Chemistry and Biophysics," *J. Phys. Chem. B*, vol. 128, no. 49, pp. 12023–12026, Dec. 2024, doi: 10.1021/acs.jpcb.4c06231.
[27] P. Szilárd, M. J. Abraham, C. Kutzner, B. Hess, and E. Lindahl, "Tackling Exascale Software Challenges in Molecular Dynamics Simulations with GROMACS," 2015, doi: 10.48550/ARXIV.1506.00716.
[28] L. Martínez, R. Andrade, E. G. Birgin, and J. M. Martínez, "P ACKMOL : A package for building initial configurations for molecular dynamics simulations," *J Comput Chem*, vol. 30, no. 13, pp. 2157–2164, Oct. 2009, doi: 10.1002/jcc.21224.

[29] B. Awawdeh, M. D'Alessio, S. Nouranian, A. Al-Ostaz, M. Ucak-Astarlioglu, and H. Alkhateb, "Molecular Dynamics Simulation of PFAS Adsorption on Graphene for Enhanced Water Purification," *ChemEngineering*, vol. 9, no. 4, p. 83, Aug. 2025, doi: 10.3390/chemengineering9040083.
[30] N. AlSawaftah, W. Abuwatfa, N. Darwish, and G. Husseini, "A Comprehensive Review on Membrane Fouling: Mathematical Modelling, Prediction, Diagnosis, and Mitigation," *Water*, vol. 13, no. 9, p. 1327, May 2021, doi: 10.3390/w13091327.
[31] P. C. B. W. Mustika, P. D. Sutrisna, S. Sutijan, H. T. B. M. Petrus, S. Sumardi, and W. Astuti, "Understanding membrane fouling in pressure-driven and thermal-driven processes for brines applications: challenges, mechanisms, characterization, mitigation strategies, and future perspectives," *Journal of Water Process Engineering*, vol. 72, p. 107631, Apr. 2025, doi: 10.1016/j.jwpe.2025.107631.
[32] S. K. Sikder, M. B. Mbanjwa, D. A. Keuler, D. S. McLachlan, F. J. Reineke, and R. D. Sanderson, "Visualisation of fouling during microfiltration of natural brown water by using wavelets of ultrasonic spectra," *Journal of Membrane Science*, vol. 271, no. 1–2, pp. 125–139, Mar. 2006, doi: 10.1016/j.memsci.2005.07.018.
[33] Y. Liu, H.-W. Li, and Z. Huang, "Editorial: Metal Hydride-Based Energy Storage and Conversion Materials," *Front. Chem.*, vol. 8, p. 675, Sep. 2020, doi: 10.3389/fchem.2020.00675.
[34] S. Homaeigohar and M. Elbahri, "Graphene membranes for water desalination," *NPG Asia Mater*, vol. 9, no. 8, pp. e427–e427, Aug. 2017, doi: 10.1038/am.2017.135.
[35] J. Zhang, Z. Xie, W. Li, S. Dong, and M. Qu, "High-capacity graphene oxide/graphite/carbon nanotube composites for use in Li-ion battery anodes," *Carbon*, vol. 74, pp. 153–162, Aug. 2014, doi: 10.1016/j.carbon.2014.03.017.
[36] Y. Qiu, B. R. Schwegler, and L.-P. Wang, "Polarizable Molecular Simulations Reveal How Silicon-containing Functional Groups Govern the Desalination Mechanism in Nanoporous Graphene," 2018, *arXiv*. doi: 10.48550/ARXIV.1804.03091.
[37] C. T. Nguyen and A. Beskok, "Charged nanoporous graphene membranes for water desalination," *Phys. Chem. Chem. Phys.*, vol. 21, no. 18, pp. 9483–9494, 2019, doi: 10.1039/C9CP01079C.
[38] D. Cohen-Tanugi and J. C. Grossman, "Water Desalination across Nanoporous Graphene," *Nano Lett.*, vol. 12, no. 7, pp. 3602–3608, Jul. 2012, doi: 10.1021/nl3012853.
[39] Y. Wang, Z. Cao, and A. Barati Farimani, "Efficient water desalination with graphene nanopores obtained using artificial intelligence," *npj 2D Mater Appl*, vol. 5, no. 1, p. 66, Jul. 2021, doi: 10.1038/s41699-021-00246-9.
[40] J. Abraham *et al.*, "Tuneable Sieving of Ions Using Graphene Oxide Membranes," 2017, doi: 10.48550/ARXIV.1701.05519.
[41] S. Wang, I. Maganga, L. Zeng, and Z. Gu, "Graphene crown pore for efficient heavy metal ion Removal: Protonated vs. Non-protonated," *Journal of Molecular Liquids*, vol. 395, p. 123819, Feb. 2024, doi: 10.1016/j.molliq.2023.123819.
[42] A. C. Lemay *et al.*, "Molecular Dynamics Simulation Prediction of the Partitioning Constants (K_H , K_{iw} , K_{ia}) of 82 Legacy and Emerging Organic Contaminants at the Water–Air Interface," *Environ. Sci. Technol.*, vol. 57, no. 15, pp. 6296–6308, Apr. 2023, doi: 10.1021/acs.est.3c00267.
[43] B. Awawdeh, M. D'Alessio, S. Nouranian, A. Al-Ostaz, M. Ucak-Astarlioglu, and H. Alkhateb, "Molecular Dynamics Simulation of PFAS Adsorption on Graphene for Enhanced Water Purification," *ChemEngineering*, vol. 9, no. 4, p. 83, Aug. 2025, doi: 10.3390/chemengineering9040083.

[44] Y.-W. Son, M. L. Cohen, and S. G. Louie, “Energy Gaps in Graphene Nanoribbons,” *Phys. Rev. Lett.*, vol. 97, no. 21, p. 216803, Nov. 2006, doi: 10.1103/PhysRevLett.97.216803.
[45] T. Wassmann, A. P. Seitsonen, A. M. Saitta, M. Lazzeri, and F. Mauri, “Structure, Stability, Edge States, and Aromaticity of Graphene Ribbons,” *Phys. Rev. Lett.*, vol. 101, no. 9, p. 096402, Aug. 2008, doi: 10.1103/PhysRevLett.101.096402.
[46] I.-C. Yeh and M. L. Berkowitz, “Ewald summation for systems with slab geometry,” *The Journal of Chemical Physics*, vol. 111, no. 7, pp. 3155–3162, Aug. 1999, doi: 10.1063/1.479595.
[47] E. Braun *et al.*, “Best Practices for Foundations in Molecular Simulations [Article v1.0],” *LiveCoMS*, vol. 1, no. 1, 2019, doi: 10.33011/livecoms.1.1.5957.
[48] J. Guénolé *et al.*, “Assessment and optimization of the fast inertial relaxation engine (fire) for energy minimization in atomistic simulations and its implementation in lammps,” *Computational Materials Science*, vol. 175, p. 109584, Apr. 2020, doi: 10.1016/j.commatsci.2020.109584.
[49] M. J. Abraham *et al.*, “GROMACS: High performance molecular simulations through multi-level parallelism from laptops to supercomputers,” *SoftwareX*, vol. 1–2, pp. 19–25, Sep. 2015, doi: 10.1016/j.softx.2015.06.001.
[50] J. A. Lemkul, “Introductory Tutorials for Simulating Protein Dynamics with GROMACS,” *J. Phys. Chem. B*, vol. 128, no. 39, pp. 9418–9435, Oct. 2024, doi: 10.1021/acs.jpcb.4c04901.
[51] B. Awawdeh, M. D’Alessio, S. Nouranian, A. Al-Ostaz, M. Ucak-Astarlioglu, and H. Alkhateb, “Molecular Dynamics Simulation of PFAS Adsorption on Graphene for Enhanced Water Purification,” *ChemEngineering*, vol. 9, no. 4, p. 83, Aug. 2025, doi: 10.3390/chemengineering9040083.
[52] T. C. Schutt, C. G. Bresnahan, T. C. Ricard, and M. K. Shukla, “Impacts of pore size in binding dynamics of per- and polyfluoroalkyl substances (PFAS) on modified graphene materials,” *Environ. Sci.: Adv.*, vol. 4, no. 10, pp. 1587–1593, 2025, doi: 10.1039/D5VA00030K.
[53] J. A, J. S Jayan, A. Saritha, S. A.S., and G. Venu, “Superhydrophobic graphene-based materials with self-cleaning and anticorrosion performance: An appraisal of neoteric advancement and future perspectives,” *Colloids and Surfaces A: Physicochemical and Engineering Aspects*, vol. 606, p. 125395, Dec. 2020, doi: 10.1016/j.colsurfa.2020.125395.
[54] A. Trifoglio *et al.*, “Tailoring graphene oxide nanosheets by alkyl amine grafting for enhanced adsorption of PFASs in drinking water: a combined theoretical and experimental study,” *Nanoscale*, vol. 17, no. 19, pp. 12124–12133, 2025, doi: 10.1039/D5NR00502G.
[55] M. Heiranian, A. B. Farimani, and N. R. Aluru, “Water desalination with a single-layer MoS2 nanopore,” *Nat Commun*, vol. 6, no. 1, p. 8616, Oct. 2015, doi: 10.1038/ncomms9616.
[56] N. Vafa *et al.*, “Graphene-Based Membranes for Water Desalination and Gas Separation: A Review of Advances in Molecular Dynamics and Machine Learning Approaches,” *Journal of Molecular Liquids*, vol. 442, p. 129092, Jan. 2026, doi: 10.1016/j.molliq.2025.129092.
[57] M. Ayala-Claveria, C. Carlesi, J. Puig, and G. Olguin, “Effects of the functionalization on the performance of graphene oxide-based membranes in the desalination and wastewater treatment: A new classification of functionalizing material,” *Chemical Engineering Journal Advances*, vol. 20, p. 100684, Nov. 2024, doi: 10.1016/j.ceja.2024.100684.
[58] J. R. Werber, C. O. Osuji, and M. Elimelech, “Materials for next-generation desalination and water purification membranes,” *Nat Rev Mater*, vol. 1, no. 5, p. 16018, Apr. 2016, doi: 10.1038/natrevmats.2016.18.
[59] N. Wei and Z. Xu, “Breakdown of Fast Water Transport in Graphene Oxides,” 2013, doi: 10.48550/ARXIV.1308.5367.

[60] A. V. Alves, M. Tsianou, and P. Alexandridis, “Fluorinated Surfactant Adsorption on Mineral Surfaces: Implications for PFAS Fate and Transport in the Environment,” *Surfaces*, vol. 3, no. 4, pp. 516–566, Sep. 2020, doi: 10.3390/surfaces3040037.
[61] L. Franck-Lacaze, P. Sistat, and P. Huguet, “Determination of the pKa of poly (4-vinylpyridine)-based weak anion exchange membranes for the investigation of the side proton leakage,” *Journal of Membrane Science*, vol. 326, no. 2, pp. 650–658, Jan. 2009, doi: 10.1016/j.memsci.2008.10.054.
[62] R. R. Nair, H. A. Wu, P. N. Jayaram, I. V. Grigorieva, and A. K. Geim, “Unimpeded Permeation of Water Through Helium-Leak–Tight Graphene-Based Membranes,” *Science*, vol. 335, no. 6067, pp. 442–444, Jan. 2012, doi: 10.1126/science.1211694.
[63] P. S. Goh, W. N. W. Salleh, N. Yusof, and A. F. Ismail, “Carbon-Based Membranes for Desalination,” in *Current Trends and Future Developments on (Bio-) Membranes*, Elsevier, 2019, pp. 27–54. doi: 10.1016/B978-0-12-813551-8.00002-4.
[64] Z. Gu, M. Duan, and Y. Tu, “Hydrophobic fluorinated graphene templated molecular sieving for high efficiency seawater desalination,” *Desalination*, vol. 523, p. 115452, Feb. 2022, doi: 10.1016/j.desal.2021.115452.
[65] M. Vaganova, I. Nesterova, Y. Kanygin, A. Kazennov, and A. Khlyupin, “Linking theoretical and simulation approaches to study fluids in nanoporous media: Molecular dynamics and classical density functional theory,” *Chemical Engineering Science*, vol. 250, p. 117383, Mar. 2022, doi: 10.1016/j.ces.2021.117383.

APPENDIX